NASA TECHNICAL NOTE

NASA TN D-4287

NASA TN D-4287

AN ANALYSIS OF THE LIMIT-CYCLE AND STRUCTURAL-RESONANCE CHARACTERISTICS OF THE X-15 STABILITY AUGMENTATION SYSTEM

by Lawrence W. Taylor, Jr., and John W. Smith

Flight Research Center
Edwards, Calif.

NATIONAL AERONAUTICS AND SPACE ADMINISTRATION • WASHINGTON, D. C. • DECEMBER 1967

NASA TN D-4287

AN ANALYSIS OF THE LIMIT-CYCLE AND STRUCTURAL-RESONANCE CHARACTERISTICS OF THE X-15 STABILITY AUGMENTATION SYSTEM

By Lawrence W. Taylor, Jr., and John W. Smith

Flight Research Center
Edwards, Calif.

NATIONAL AERONAUTICS AND SPACE ADMINISTRATION

For sale by the Clearinghouse for Federal Scientific and Technical Information
Springfield, Virginia 22151 – CFSTI price $3.00

AN ANALYSIS OF THE LIMIT-CYCLE AND STRUCTURAL-RESONANCE CHARACTERISTICS OF THE X-15 STABILITY AUGMENTATION SYSTEM

By Lawrence W. Taylor, Jr., and John W. Smith
Flight Research Center

SUMMARY

During the early flights of the X-15 airplane, two problems associated with the stability augmentation system were encountered: limit cycles, primarily in roll, and control-surface resonance. The limit cycles were usually only an annoyance to the pilot, but at flight conditions with the largest control power, the nature of the limit cycles changed abruptly to large-amplitude oscillations that could have caused complete loss of control. The frequency and amplitude of the airplane-system limit cycles were calculated by using the describing-function technique together with a nonlinear mathematical model to represent the control system and the airplane. These calculated characteristics compared well with experimental results from flight, ground tests, and simulations. The calculations were repeated for two different electronic filters, the original and a subsequent, improved design, that were incorporated in the stability augmentation system. The calculated limit-cycle characteristics for the final filter did not agree as well with experimental results as did the characteristics calculated for the original filter.

The second problem, a structural resonance induced by the stability augmentation system, was experienced only after the electronic filter was changed. This problem was analyzed by representing the flexible horizontal stabilizers as a spring-mass system and the airplane as a rigid body. The calculated critical gains were about a factor of three lower than those obtained experimentally from ground tests. An analysis was also made in which the right and left damper channels were assumed to have unequal gains in order to explain an interdependency between the roll and pitch axes evident in the experimental results.

INTRODUCTION

Although the stability augmentation system (SAS) of the X-15 airplane is simple in concept, some difficulties have been encountered as a result of hysteresis in control linkages and low structural damping of the control surfaces. The phase lag attributed to hysteresis and other nonlinearities caused SAS-induced limit cycles which were generally only bothersome to the pilot but could cause loss of control at the extremes of the flight envelope. Efforts to alleviate the limit-cycle problem by reducing the amount of hysteresis were not successful; therefore, an electronic filter in the SAS

was modified to reduce the phase lag in the system. As a result, the limit-cycle problem was significantly alleviated. Initial flight tests indicated the modified filter to be satisfactory. A resonance problem still existed during ground tests, however, which made it necessary to reduce the SAS gains while the airplane was on the ground.

During a subsequent flight to an altitude of 170,000 feet (51,800 meters), a severe in-flight vibration of approximately 13 cps was encountered. The vibration onset occurred at a Mach number of 4 and a dynamic pressure of 100 lb/ft^2 (4788 N/m^2) as the pilot prepared for reentry. The vibration continued for almost a minute, at which time the pilot reduced the pitch SAS gain. The dynamic pressure during the vibration period reached a maximum value of 980 lb/ft^2 (46,900 N/m^2). The oscillograph record of this portion of the flight showed a 13-cps oscillation on all channels. The vibration was limited in amplitude because of the rate limit (25 deg/sec) of the surface actuator; however, the surface deflections at 13 cps were about 1° peak to peak. No serious damage is known to have resulted from the vibration, although during postflight inspection the horizontal-stabilizer bearing surfaces were found to be scored.

As a result of the flight experience with the modified filter, it was clear that both problems would have to be considered simultaneously in the selection of an acceptable filter. These problems were discussed broadly in references 1 to 3, but the comprehensive analysis required to solve the problems has not been published. This paper considers in some detail the limit-cycle and structural-resonance problems by using nonlinear mathematical models in the analysis of the system stability. The results of the analysis are compared with results obtained from ground and flight tests. Limit-cycle calculations involved multiple, nonseparable, nonlinear elements which demonstrate the use of describing functions (ref. 4). The structural-resonance problem was a variation of the more classical structural-feedback problem (ref. 5). Although this paper is primarily concerned with the X-15 stability augmentation system, the techniques of analysis, the ground tests, and the correlation between calculated and experimental characteristics are applicable to many vehicles with high-gain control systems.

SYMBOLS

Measurements for this investigation were taken in the U.S. Customary System of Units. Equivalent values are indicated in the International System of Units (SI) in the interest of promoting use of this system in future NASA reports. Details concerning the use of SI, together with physical constants and conversions, are given in reference 6.

A	structural-feedback gain in roll,	$\frac{\int m_h(x - x_{HL})ydm}{I_X}$
A(s)	structural-feedback dynamics in roll	
B	structural-feedback gain in pitch,	$\frac{\int m_h(x - x_{HL})xdm}{I_Y}$

$B(s)$	structural-feedback dynamics in pitch
D	dead-band total amplitude, degrees
$e_{-2} \ldots e_4$	peak-to-peak signal amplitude having both amplitude and phase (see fig. 5), degrees
f	frequency, cycles per second
G_D	sinusoidal describing function
H	total width of hysteresis, degrees
h	altitude, feet (meters)
I_X	moment of inertia of the airplane about the X-axis, slug-foot^2 (kilogram-meter^2)
I_Y	moment of inertia of the airplane about the Y-axis, slug-foot^2 (kilogram-meter^2)
I_Z	moment of inertia of the airplane about the Z-axis, slug-foot^2 (kilogram-meter^2)
$j = \sqrt{-1}$	
K	gain of nonlinearity
K_p	roll-damper gain, degree/degree/second
K_q	pitch-damper gain, degree/degree/second
K_r	yaw-damper gain, degree/degree/second
L_p	roll damping, $\frac{\text{Moment per } p}{I_X}$, radians/second^2/radians/second
$L(s)$	dynamics of left channel (left horizontal stabilizer)
L_{δ_a}	roll control power, $\frac{\text{Moment per } \delta_a}{I_X}$, radians/second^2/radian
M	zero to peak amplitude of a sinusoidal input of a nonlinear element, degrees
M_{δ_h}	pitch control power, $\frac{\text{Moment per } \delta_h}{I_Y}$, radians/second^2/radian

m	mass, slugs (kilograms)
m	input to nonlinear element, degrees
N	zero to peak amplitude of the sinusoidal portion of the output of a nonlinear element, degrees
N_{δ_r}	yaw control power, $\frac{\text{Moment per } \delta_r}{I_Z}$, radians/second^2/radian
n	output of nonlinear element, degrees
P	static atmospheric pressure, pounds/foot^2 (newtons/meter^2)
p	roll rate, radians/second
q	pitch rate, radians/second
R(s)	dynamics of right channel (right horizontal stabilizer)
r	yaw rate, radians/second
S	saturation limit, degrees
s	Laplace variable
X, Y, Z	airplane roll, pitch, and yaw body axes, respectively
x	distance along X-axis
y	distance along Y-axis
Δq	pitch-rate limit-cycle amplitude, peak to peak, degrees/second
Δr	yaw-rate limit-cycle amplitude, peak to peak, degrees/second
$\Delta\zeta_h$	aerodynamic damping of the horizontal-stabilizer structural mode
$\Delta\varphi$	bank-angle limit-cycle amplitude, peak to peak, degrees
δ_a	"aileron" or total differential horizontal-stabilizer deflection, degrees
δ_h	"elevator" or average horizontal-stabilizer deflection, degrees
δ_r	rudder deflection, degrees
ζ	damping ratio of the airplane

ζ_h	damping ratio of first structural mode of the horizontal stabilizers
σ	real part
ω	frequency, radians/second
ω_n	natural frequency, radians/second
ω_{n_θ}	short-period natural frequency in pitch, radians/second
ω_{n_ψ}	Dutch roll natural frequency, radians/second
$\lvert\ \rvert$	amplitude ratio or absolute value
$\angle$	phase angle, degrees

Subscripts:

HL	hinge line
h	horizontal stabilizers
LC	limit cycle
N	nonlinear
θ	pitch
ψ	yaw

A dot over a quantity denotes a derivative with respect to time.

DESCRIPTION OF AIRPLANE AND ASSOCIATED EQUIPMENT

X-15 Airplane

The X-15 airplane (fig. 1) is a single-place, rocket-powered vehicle designed and built by North American Aviation, Inc., for the U.S. Air Force and NASA for research and development purposes. It has a low-aspect-ratio wing and high wing loading. The X-15 was designed to reach a Mach number of 6 and altitudes greater than 250,000 feet (76,200 meters). The airplane is constructed primarily of welded and riveted Inconel X. Directional control is obtained by deflecting the all-movable portions of both the upper and lower vertical stabilizers. Recent flights have been made with the lower rudder removed. Pitch control is obtained by moving the horizontal stabilizers together, and roll control by moving them differentially.

Figure 2 is a simplified sketch of the longitudinal control system; the other axes are similar. The pilot input is transmitted through a series of bellcranks and cables

to the walking beams which serve as mechanical summers for SAS and pilot inputs. The outputs of the walking beams then go to the valve arms of the control-surface actuators.

Stability Augmentation System

The X-15 stability augmentation system was designed by the Westinghouse Electric Corp., to North American Aviation, Inc., specifications. The essential components of the system, as shown in figure 3, are gyros, cockpit gain selectors, electronic case assemblies, and servos. The outputs of the servos go to their respective control-surface actuators after being summed with the pilot input. Gain selectors are provided to enable the pilot to change the gain during flight. In addition to the normal damper loops, a crossfeed is provided in which the yaw-rate signal is summed with the roll-rate signal. This feature is used to improve airplane stability at high angles of attack when the lower rudder is installed.

The gain values that correspond to the various gain-selector settings are given in the following table:

Gain-selector position	Gain, deg/deg/sec			
	Pitch	Roll	Yaw	Yar
1	0.075	0.05	0.03	0.09
2	.150	.10	.06	.18
3	.225	.15	.09	.27
4	.300	.20	.12	.36
5	.375	.25	.15	.45
6	.450	.30	.18	.54
7	.525	.35	.21	.63
8	.600	.40	.24	.72
9	.675	.45	.27	.81
10	.750	.50	.30	.90

A more detailed description of the control system is presented in reference 2.

Flight Simulator

During the early design of the X-15 airplane, a six-degree-of-freedom flight simulation was used in conjunction with analytical predictions to determine the control-system requirements. Subsequently, the flight simulator was used for flight planning, pilot training, and control-system development, as reported in reference 7. The flight simulator, pictured in figure 4, consists of an almost identical layout of the X-15 cockpit, control cables, linkages, and actuators. Dummy control surfaces were used. An extensive simulation of the aircraft flight dynamics is provided by an analog computer. Control-system modifications can be realistically tested on the simulator before being installed in the actual airplane.

TEST PROCEDURES

Flight Tests

Theoretically, a small control disturbance is required to excite limit cycles in flight; however, the normal motion of the X-15 airplane was sufficient to excite the limit cycles. Since the occurrence and amplitude of limit cycle depended on control power, the selection of flight conditions required some consideration for flight safety. For example, the combination of high dynamic pressure and angle of attack that occurs during the recovery of the X-15 from a flight to high altitude results in large values of control power. Consequently, these flight conditions were critical with respect to limit cycles. The critical nature of the reentry maneuver precluded its use to investigate limit cycles. As a result, the powered, climbout portion of flight was modified so that high values of dynamic pressure could be obtained. The limit-cycle characteristics were checked at the highest products of system and airplane gains deemed necessary.

Normal pilot control inputs during reentry from high altitude were sufficient to excite the structural resonance, so no specific tests were required.

Ground Tests

The term "ground tests" is used to denote integrated tests in which the X-15 airplane, airplane control systems, and an analog computer were used. During the limit-cycle tests, the analog computer provided a simulation of the aerodynamic loops, one at a time, by computing the aircraft response that results from the deflection of the control surfaces.

The transfer functions mechanized on the analog computer were as follows:

$$\frac{p(s)}{\delta_a(s)} = \frac{-L_{\delta_a}}{L_p - s}$$

$$\frac{q(s)}{\delta_h(s)} = \frac{M_{\delta_h} s}{s^2 + 2\zeta_\theta \omega_{n_\theta} s + \omega_{n_\theta}{}^2}$$

$$\frac{r(s)}{\delta_r(s)} = \frac{N_{\delta_r} s}{s^2 + 2\zeta_\psi \omega_{n_\psi} s + \omega_{n_\psi}{}^2}$$

The structural-resonance ground tests were performed with the X-15 airplane on a rubber-tired dolly in an effort to make the frequency associated with the support of the airplane as low as possible. The response of the airplane in the range of frequencies near that of the control-surface resonance then should have been the same as in flight and thus could be studied under controlled conditions. The analog computer was

not needed to compute airplane response, as for the limit-cycle tests, but was used to mechanize various filters and to enable higher levels of gain to be investigated than would otherwise have been available. The resonance could be triggered by either abrupt or continuous movement of the control stick.

Frequency-response measurements were made of the servo and surface actuators at a large variety of amplitudes to enable formulation of a nonlinear mathematical model.

Flight-Simulator Tests

The X-15 flight simulator incorporates a nearly exact duplicate of the actual control-system components and hardware and so is ideally suited for use as a test bed for designing, checking, and performing system tests. In studying limit-cycle characteristics, the equations of motion were reduced from the usual six degrees of freedom to five degrees of freedom by making speed invariant. This enabled tests to be made at a fixed, preselected flight condition. No other changes were necessary, inasmuch as a complete SAS was available as a part of the simulator. The limit cycles were allowed to reach much larger amplitudes on the flight simulator than could be tolerated by the actual airplane.

The horizontal-stabilizer surface-resonance phenomenon was also studied on the simulator by providing an additional feedback loop that represented the inertial reaction of the fuselage to the vibrating horizontal stabilizer. This was done by installing strain gages on the roots of the beams which simulated the horizontal stabilizers. Only the first structural mode was simulated, however. The outputs from the strain gages provided a signal proportional to the reaction of the fuselage as if it were free to move. By simulating the inertial loop in this way, a number of system tests could be performed that otherwise could not have been accomplished because of the possibility of damage to the airplane.

METHODS OF ANALYSIS

The limit-cycle and structural-resonance problems involving the X-15 stability augmentation system were analyzed by utilizing sinusoidal describing functions and strictly linear system theory, respectively. Although it was necessary to consider the two problems simultaneously in the selection of a filter for the SAS, the analyses are treated separately. The success of the analyses in terms of correlation with experimental results is discussed in a subsequent section.

Limit Cycles

Ideally, the X-15 stability augmentation system would completely damp the transient motion of the airplane if pilot input were constant. However, the X-15 control system has considerable hysteresis because of the accumulated free play of the large number of mechanical linkages (ref. 2). In addition, there are nonlinearities in the surface actuator in the form of rate limiting and valve overlap. With these system

characteristics, the airplane motions for many flight conditions will subside only to a continuing oscillation.

As the magnitude of the applied control is reduced and approaches the size of the hysteresis, the phase and amplitude relationships change markedly. Consequently, it is possible to experience sufficient additional phase lag to cause the damper control action to sustain the airplane motion.

Nonlinear actuator. – A mathematical model of the nonlinear portion of the X-15 control-system actuator was constructed using sinusoidal describing functions as shown in figure 5. The characteristic values of the nonlinear elements were selected to match experimental data, including frequency-response results. Since the limit cycle is essentially sinusoidal, it is possible to relate input and output of each of the nonlinear elements with sinusoidal describing functions. By knowing the vector relationship across each of the nonlinear elements, the output-to-input relationship across the whole model can be determined (ref. 4). For example, the input to the second hysteresis element in figure 5 may be specified and the magnitude and phase of the signal traced through the forward loop until the model output is reached. The input to the model can then be obtained by working back through the feedback loop, the summing junction, and the first hysteresis element, thus establishing the relationship between the input and the output.

A typical calculation was as follows:

1. With reference to figure 5, specify e_0 and f. For example, let $|e_0| = 3.0$, $\angle e_0 = 0°$, and $f = 1.0$ cps.

2. Determine e_1 by using figure 6(a) where the ratio of hysteresis to input amplitude (peak to peak) $\frac{H}{2|M|} = \frac{H}{|e_0|} = \frac{0.3}{3.0} = 0.1$ which gives $\frac{|G_D|}{K} = 0.95$ and $\angle G_D = -6°$. Then

$$|e_1| = \frac{|e_0||G_D|}{K} = (3.0)(0.95) = 2.85$$

$$\angle e_1 = \angle e_0 + \angle G_D = 0° + (-6°) = -6°$$

3. Next, determine the output of the saturation using figure 6(b), where

$$\frac{S}{K|M|} = \text{ratio of saturation level to input (zero to peak)}$$

where

$$S = 1.0 \text{ and } K = 1.0$$

$$\frac{S}{K|M|} = \frac{S}{K\frac{|e_1|}{2}} = \frac{1.0}{\frac{(1.0)(2.85)}{2}} = 0.704$$

so

$$\frac{|G_D|}{K} = 0.81 \text{ and}$$

$$|e_2| = |e_1|\frac{|G_D|}{K} = (2.85)(0.81) = 2.3$$

Since there is no change in phase,

$$\angle e_2 = \angle e_1 = -6°$$

4. Next, determine the output of the dead band by using figure 6(c), where

$$\frac{D}{2|M|} = \frac{D}{|e_2|} = \frac{0.05}{2.3} = 0.0217$$

and

$$\frac{|G_D|}{K} = 0.97$$

$$|e_3| = |e_2| \frac{|G_D|}{K} = (2.3)(0.97) = 2.2$$

Since there is no change in phase,

$$\angle e_3 = \angle e_2 = -6°$$

5. Next, determine the output of the hydraulic cylinder by using the following expression:

$$|e_4| = \frac{|e_3|\,25}{|s|} = \frac{|e_3|\,25}{2\pi f} = \frac{(2.2)(25)}{(6.28)(1.0)} = 8.8$$

Since a 90° phase lag is introduced,

$$\angle e_4 = \angle e_3 - 90° = -96°$$

6. The output of the first hysteresis is determined by finding the input to the summing point as follows:

$$e_0 = e_{-1} - e_4$$

or

$$e_{-1} = e_0 + e_4$$

Therefore,

$$|e_{-1}| = \sqrt{(|e_0| + |e_4| \cos \angle e_4)^2 + (|e_4| \sin \angle e_4)^2} = \sqrt{[3 + 8.8 \cos (-96°)]^2 + [8.8 \sin (-96°)]^2}$$

$$|e_{-1}| = 9.02$$

and the phase angle

$$\angle e_{-1} = \tan^{-1}\left[\frac{8.8 \sin(-96°)}{3 + 8.8 \cos(-96°)}\right] = -71.5°$$

7. The input to the first hysteresis is determined by using figure 6(d), which shows the hysteresis describing function arranged to enable computing the input by knowing the output where

$$\frac{2|N|}{KH} = \frac{9.02}{0.3} = 30$$

and

$$\frac{|G_D|}{K} = 0.99$$

$$|e_{-2}| = \frac{|e_{-1}|}{\frac{|G_D|}{K}} = \frac{9.02}{0.99} = 9.1$$

$$\angle e_{-2} = \angle e_{-1} - \angle G_D = -71.5° - 3.0° = -74.5°$$

8. Finally, the ratio of output to input is obtained as

$$\frac{|e_4|}{|e_{-2}|} = \frac{8.8}{9.1} = 0.97$$

and

$$\angle \left(\frac{e_4}{e_{-2}}\right) = \angle e_4 - \angle e_{-2} = -96° + 74.5° = -21.5°$$

By repeating these calculations a number of times for the frequency range of interest, functions shown in figures 7(a) and 7(b) can be determined. These functions relate the output to the input of the nonlinear model of the control system. After these relationships have been determined, limit-cycle characteristics can be calculated.

Roll limit cycles. – For the X-15 roll limit cycles, the following greatly simplified transfer function relating roll rate to aileron deflection can be used:

$$\frac{p(s)}{\delta_a(s)} = \frac{L_{\delta_a}}{s}$$

Note that the s term in the denominator contributes a phase-angle lag of 90° between roll rate and aileron deflection. The simplification is conservative in that aerodynamic damping would reduce the phase lag slightly. Thus, the remaining 90° of phase lag necessary for a continuing oscillation will come from the electronic filter and power actuator. The calculated nonlinear actuator characteristics (fig. 7) and the Bode plot of the electronic filter (fig. 8) are used in the following steps in calculating the limit-cycle characteristics:

1. Select a frequency.

2. Read from figure 8 the phase angle and amplitude ratio of the electronic filter.

3. Read from figure 7 the amplitude $|e_{-2}|$ and the amplitude ratio $\left|\frac{e_4}{e_{-2}}\right|$ that correspond to the frequency and complement the filter phase lag obtained in step 2; that is, $\angle_N = -90° - \angle_{filter}$.

4. Compute overall gain from the expression

$$K_p L_{\delta_a} = \frac{2\pi f}{||_{filter} \, ||_{actuator}}$$

5. Compute limit-cycle amplitude times roll gain from the expression

$$K_p \Delta\varphi = \frac{|e_{-2}|}{||_{filter} 2\pi f}$$

6. Repeat for other frequencies.

The quantities $K_p L_{\delta_a}$ and $K_p \Delta\varphi$ are computed to make it possible to present all the limit-cycle characteristics on two curves. Otherwise, two families of curves would be required. Figure 9 shows example plots of $K_p \Delta\varphi$ and $K_p L_{\delta_a}$ versus frequency that were calculated by using the procedure outlined above.

Pitch and yaw limit cycles. – Limit cycles in pitch and yaw are different from those in roll because the frequency range is usually lower and more limited. (If not, a model analogous to the roll axis can be used.) Consequently, the effect of frequency variance on the actuator characteristics is very slight, thus enabling a simplified description to be used. The description of the nonlinear characteristics of the amplitude and phase of the actuator loop is presented in figure 10 as a function of input amplitude $|e_{-2}|$. This description of the nonlinear control system, plus a transfer function which relates pitching velocity to surface deflection, is all that is needed to compute limit-cycle characteristics for the pitch case. The transfer function used for the airplane dynamics is

$$\frac{q(s)}{\delta_h(s)} = \frac{M_{\delta_h} s}{s^2 + 2\zeta_\theta \omega_{n_\theta} s + \omega_{n_\theta}^2}$$

By placing this function into the damper loop, along with the nonlinear element, the total system can be depicted as shown in the sketch on the following page.

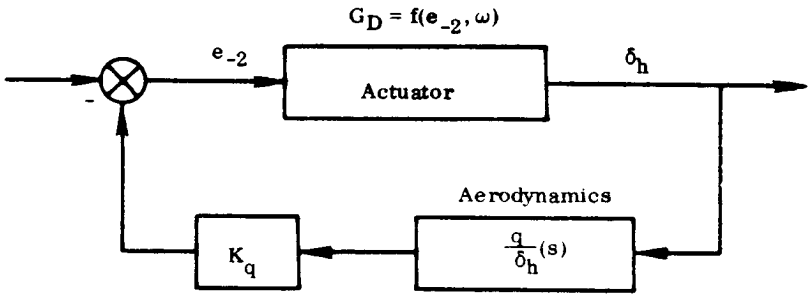

The necessary conditions for limit-cycle oscillations are a phase shift of -180° and total loop gain of unity. The limit-cycle frequency in pitch will be closely related to ω_{n_θ} because of low damping, which results in a very large change in the phase lag of the airplane at the natural frequency (fig. 11). For this reason, a frequency ratio $\frac{\omega}{\omega_{n_\theta}}$ and the gain parameter $\frac{K_q M_{\delta_h}}{\omega_{n_\theta}}$ are used in the limit-cycle parameterization. For example, substituting $j\omega$ for s in

$$K_q \frac{q(s)}{\delta_h(s)} = \frac{K_q M_{\delta_h} s}{s^2 + 2\zeta_\theta \omega_{n_\theta} s + \omega_{n_\theta}{}^2}$$

yields

$$K_q \frac{q(\omega)}{\delta_h(\omega)} = \frac{K_q \left(\frac{M_{\delta_h}}{\omega_{n_\theta}}\right) \frac{j\omega}{\omega_{n_\theta}}}{1 - \left(\frac{\omega}{\omega_{n_\theta}}\right)^2 + 2j\zeta_\theta \frac{\omega}{\omega_{n_\theta}}}$$

Then $\frac{K_q M_{\delta_h}}{\omega_{n_\theta}}$ would be a logical choice of gain parameter since it is the gain given by the Bode plot asymptote at ω_{n_θ}. The limit-cycle amplitude parameter that is used is the damper gain times the peak-to-peak pitch or yaw rate. Multiplication by the damper gain results in a quantity that is directly related to the input of the nonlinear portion of the control system. Consequently, the number of plots needed to summarize the limit-cycle characteristics is greatly reduced.

The method used to compute the limit-cycle characteristics for pitch and yaw is as follows:

1. Select values for ζ_θ and $\frac{\omega}{\omega_{n_\theta}}$. Read from figures 11(a) and 11(b) the corresponding amplitude ratio and phase angle.

2. Read from figure 10(b) the amplitude e_{-2} which gives the supplement of the phase angle $\angle \frac{\delta_h}{e_{-2}}$ read in step 1; that is, phase angle = -180° + second-order phase angle.

3. Knowing e_{-2}, obtain the amplitude ratio $\left|\frac{\delta_h}{e_{-2}}\right|$ from figure 10(a).

4. To meet the requirement for unity loop gain

$$\frac{K_q M_{\delta_h}}{\omega_{n_\theta}} = \frac{1}{\frac{\omega}{\omega_{n_\theta}}\left|\frac{\delta_h}{e_{-2}}\right|\left|\frac{1}{\left(\frac{j\omega}{\omega_{n_\theta}}\right)^2 + 2\zeta_\theta\left(\frac{j\omega}{\omega_{n_\theta}}\right) + 1}\right|}$$

where e_{-2} is the amplitude, $K_q\Delta q$ or $K_r\Delta r$, that enables a solution.

Obtaining a number of solutions by using a digital computer generates the curves presented in figure 12. This final plot predicts the limit cycles where the overall gain would be $\frac{K_q M_{\delta_h}}{\omega_{n_\theta}}$ or $\frac{K_r N_{\delta_r}}{\omega_{n_\psi}}$. However, the transfer function, as such, to represent the airplane is less accurate for yaw because of the coupling between roll and yaw.

Structural Resonance

When the electronic filter of the SAS was modified to improve the characteristics of the limit cycles, a severe vibration was encountered in which the SAS caused the horizontal stabilizers to resonate at their first (bending) natural frequency. The modified filter had less phase lag, but, more important, the gain at the first natural frequency of the horizontal stabilizer was increased by about a factor of three, giving rise to the structural-resonance problem.

One mechanism by which this resonance phenomenon can be explained is shown in figure 13. The vibrating surfaces, represented in the figure by masses at the ends of flexible beams, caused the relatively rigid but freely supported airplane to oscillate at a small but perceptible amplitude. This motion was sensed by the SAS rate gyros, and signals were sent to the servos to damp the motion. However, the accumulated phase lag at these frequencies was large and the SAS input only served to sustain the vibration.

Roll mode. – Figure 13 also shows a block diagram of the inertial loop and the aerodynamic loop for the X-15 roll mode. It is assumed that bending of the horizontal stabilizer does not alter the aerodynamic moment. This is a reasonable assumption because of the very slight effect of bending on the angle of attack of the stabilizer and because of the high frequencies involved. The gain A of the inertial loop can be formulated by considering the force needed to accelerate an infinitesimal mass in order to relate the second derivative of the surface deflection to a moment about the roll axis. This result is then integrated over the mass of the horizontal stabilizer as follows:

$$A = \int_{m_h} \frac{(x - x_{HL})y\,dm}{I_X}$$

From the block diagram, the characteristic equation is

$$K_p\left[L_{\delta_a}+\frac{As^2}{\left(\frac{s^2}{80^2}+\frac{2\zeta_h s}{80}+1\right)}\right]\frac{1}{s\left(\frac{s^2}{180^2}+\frac{0.8s}{180}+1\right)^3(1+0.15s)}+1=0$$

The root locus of the above expression with the L_{δ_a} aerodynamic loop term eliminated is shown in figure 14. As the loop gain is increased, the structural mode becomes less damped and goes unstable. Since the resonant frequency nearly equals the natural frequency of the structure, it is possible to obtain a simple expression for the critical gain by substituting j80 for s, as

$$K_{p_{critical}}=\frac{656}{L_{\delta_a}+\frac{3200A}{\zeta_h}}\approx 14.1\zeta_h$$

Note that ζ_h is the total damping of the structural mode (see fig. 15 and ref. 8). After the values, $L_{\delta_a}=120$, which was most adverse, and $A=0.0145$ and $\zeta_h=0.005$, which are representative values, are substituted into this expression, it is apparent that the contribution of the aerodynamic loop is negligible when compared to the inertial loop even for the most adverse values of L_{δ_a} and ζ_h. The contribution of the inertial loop is greater than 98 percent of the total gain necessary to drive the system unstable. Also, from the above expression, it is evident that the critical gain is proportional to the structural damping ratio of the horizontal stabilizer. Unfortunately, the value of damping ratio is not accurately known, but it has been estimated to be 0.005.

It is known that the structural damping of an aerodynamic surface may be altered by its aerodynamic environment. The effect of the aerodynamic environment on the structural damping is estimated to be $\Delta\zeta_h=54P$ for Mach numbers greater than 2.0 (ref. 8). An estimate of the combined structural and aerodynamic damping ratio for the horizontal stabilizer as a function of altitude is presented in figure 15. The decrease in damping with increasing altitude is clearly shown, which implies that the critical SAS gain which causes structural resonance decreases as altitude is increased.

Pitch mode. – The structural-resonance problem with the X-15 airplane is almost as serious in the pitch mode as in the roll mode. The block diagram of figure 13 is also representative of the pitch mode if the coefficients A, K_p, and L_{δ_a} are replaced by B, K_q, and M_{δ_h}, respectively. The maximum value of M_{δ_h} is 50, which makes the aerodynamic gain in pitch less significant than the aerodynamic gain in roll. The critical gain in pitch is 0.105 deg/deg/sec, which is surprisingly close to the critical gain in roll of 0.07 deg/deg/sec.

Combined pitch and roll modes. – Figure 16 shows a block diagram for the simultaneous consideration of both pitch and roll. The resulting characteristic equation is

$$1 + \frac{1}{2}[A(s)K_p(s) + B(s)K_q(s)][L(s) + R(s)] + A(s)B(s)K_p(s)K_q(s)L(s)R(s) = 0$$

which, if $R(s) = L(s)$, reduces to

$$[1 + A(s)K_p(s)L(s)][1 + B(s)K_q(s)L(s)] = 0$$

It is evident from the factored form of the characteristic equation that the roll and pitch modes are independent and give the same critical gains that were obtained by examining each axis separately.

Figure 17 is a plot of pitch gain versus roll gain on which critical gains can be shown. The rectangular boundary depicts the condition of independent pitch and roll axes and represents complete symmetry for the right and left channels of the control system ($L(s) = R(s)$). If the channels are not symmetrical ($L(s) \neq R(s)$), the critical gains must be determined from the coupled, unfactored characteristic equation. Two examples are shown in figure 17, one for the gain of one side equal to zero, and the other for the gain of one side equal to one-half that of the other side. It is noted that if the gain of either side (channel) remains constant, all the boundaries have a point in common. At this point the critical gain is not changed, although the gain is reduced in either the right or left (not both) channels.

RESULTS AND DISCUSSION

Flight, ground, and simulator tests were conducted to define the airplane–system characteristics and to assess possible changes to improve the operation of the system. The results of these tests are compared with computed characteristics based on the analyses described in the preceding section. Comparisons are made between theory and experiment with a view to extending the use of the analysis beyond the X-15 airplane.

Original Filter

The original SAS filter was second order with a break frequency of 10 cps. It was designed to improve the overall operation of the system by attenuating the gain at high frequencies; however, limit cycles were observed on the simulator and in flight. To gain some insight into the limit cycle experienced with this filter, an analysis was first performed with the aid of describing functions. One result of the analysis was the identification of the independent parameters and an indication of their relative importance. By using three independent parameters, for example, the limit-cycle characteristics in roll can be summarized by two functions of two variables each instead of two functions of three variables each. Figure 18 compares the limit-cycle characteristics in roll obtained from various tests with calculated characteristics. "Ground test" in

figure 18 refers to a simulation of the aerodynamic loop $\left(\frac{p(s)}{\delta_a(s)} = \frac{L_{\delta_a}}{s}\right)$ by using an analog computer to provide the X-15 airplane flight dynamics. The correlation shown is considered to be good for a phenomenon that is dependent on hysteresis, a quantity subject to wear and adjustment. Note that as the effective gain $K_p L_{\delta_a}$ increases, the limit cycle frequency becomes multivalued. The "jump" phenomenon was verified on the flight simulator. Theoretically, it is possible to jump anywhere in the multivalued range, but in practice the jump occurs only at the larger values of $K_p L_{\delta_a}$ shown.

The jump does not occur instantaneously, as the term implies, but takes several seconds, as can be seen in the simulator time history in figure 19. The motion caused by the limit cycle beyond the jump was large in amplitude and could cause loss of control of the airplane and extreme stresses to the airplane and control hardware. Even ground testing was minimized. The flagged symbols in figure 18 designate the transient values of the limit-cycle amplitude. The flight conditions that caused the dangerous change in roll limit-cycle amplitude were at the very edge of the X-15 flight envelope. The flight envelope was necessarily restricted until an improved electronic filter was available.

Modified Filter

The modified electronic filter consisted of a high-pass filter with a corner frequency above 30 cps; the corner frequency of the original filter was about 10 cps. This modification reduced the roll limit-cycle amplitudes at the most adverse flight conditions by reducing the phase lag of the electronic filters. The roll limit-cycle characteristics of the modified filter are compared with those of the original filter in figure 20. The limit-cycle amplitudes were reduced, particularly at the larger values of $K_p L_{\delta_a}$. More important, the critical value of $K_p L_{\delta_a}$ at which the limit-cycle amplitude changed drastically was increased to a value outside the X-15 flight envelope.

The use of the modified filter effectively reduced the limit-cycle amplitude; however, another problem, horizontal-stabilizer resonance, was thereby encountered. The source of the resonance was traced to a threefold increase in the system gain at the natural frequency of the horizontal-stabilizer bending mode as a result of substituting the modified filter. In the analysis it was predicted that the SAS could cause resonance at pitch or roll gains of 0.105 or 0.07, respectively. Ground tests indicated, however (fig. 21), that about three times these gain values would be necessary to sustain resonance. Because of the nature of the problem, better agreement would not be anticipated. In addition, special tests were made to check the model used to describe the inertial loop. Figure 22 compares calculated and measured frequency response of roll rate due to surface deflection. The transfer function relating roll rate to surface deflection used in the analysis was

$$\frac{p(s)}{\delta_a(s)} = \frac{As}{\left(\frac{s^2}{80^2} + \frac{0.01s}{80} + 1\right)}$$

This expression was obtained by considering the inertial reaction to roll control-surface deflections (fig. 13). For these calculations the following values were used: structural feedback gain, $A = 0.0145$; horizontal-stabilizer natural frequency, $\omega_{n_h} = 80$ radians/second; and horizontal-stabilizer structural damping, $\zeta_h = 0.005$.

The experimental data (fig. 22) were obtained with the airplane mounted on a rubber-tired dolly which supports the aft end of the airplane during ground operations. Manual control inputs to the horizontal-stabilizer control surfaces were used to excite the natural bending frequency of the surfaces. Although the data points obtained were slightly higher than the calculated curve, the data are believed to validate the model used in the analysis. The number of data points is limited, since the data were obtained under resonance conditions.

Notch Filter

System stability problems with the original and modified filters led to the design of still another filter for the stability augmentation system. The goals of this design were to reduce the roll limit-cycle amplitudes and to avoid the surface resonance problem encountered with the modified filter. A calculated frequency-response comparison of the three filters is presented in figure 23.

With the notch filter, the phase lag in the frequency range of 2 cps to 6 cps was less than that for the original filter, which thereby reduced the limit-cycle amplitude but not to the extent obtained with the modified filter. In figure 24, calculated and measured roll limit-cycle amplitudes are compared for a variety of experimental tests with the notch filter. In general, the experimental results are underpredicted by the describing-function method of analysis. However, with the notch filter, the critical value of $K_p L_{\delta_a}$ was increased to a value in excess of that normally encountered (approximately 36) within the flight envelope of the X-15 airplane.

As shown in figure 23, the attenuation of roll-amplitude ratio at 13 cps with the notch filter was greater than with the other two filters. In fact, at the critical frequency, the modified filter had a gain increase which necessitated an overall operating gain reduction to avoid stabilizer resonance. An analysis showed that the notch filter increased the gain margin by a factor of about 10. This increase was confirmed by ground tests which demonstrated stability at gains twice the maximum value available in flight. The gains of all the filters were not materially affected at the lower frequencies that are important for airplane handling considerations.

Pressure-Feedback Valve

In an attempt to solve the resonance problem mechanically by providing artificial damping to the resonant surface, a pressure-feedback valve was designed and constructed. Since the difference in pressure across the piston is proportional to the inertial loading and since the piston deflection is the integral of valve deflection, it seemed reasonable to use the pressure difference as a feedback signal to the valve. An analysis of the effect of the valve on the resonance problem is included in reference 8. The valve and the original X-15 actuator cylinder were installed on the X-15 flight simulator. Tests revealed excessive valve friction, with the result that an

input to the SAS on the order of 1 cps produced no actuator response. Instead, the input was transmitted through the control-system linkage to the cockpit. The development of the pressure-feedback valve was discontinued after unsuccessful attempts were made to reduce the valve friction.

CONCLUDING REMARKS

Two problems associated with the X-15 stability augmentation system were encountered during early flights of the vehicle. They were limit cycles, principally in roll, and control-surface resonance. A systems analysis was made of both problems, and the calculated critical gains, limit-cycle amplitudes, and frequencies were compared with analog simulation and flight results.

The X-15 stability augmentation system causes the airplane to oscillate at a small amplitude and at frequencies up to 3 cps. These limit cycles are most noticeable in roll and are caused by the phase lag of hysteresis and other nonlinearities in the mechanical portion of the control system. Although, in general, the limit cycles are only annoying to the pilot, a potentially dangerous situation existed with the original electronic filter. Analysis and experience showed that the limit-cycle amplitude in roll abruptly increased at certain values of loop gain $K_p L_{\delta_a}$ and could cause loss of control.

A nonlinear, mathematical model of the actuator and linkages was used successfully to gain an understanding of the limit-cycle problem and to calculate limit-cycle amplitudes and frequencies. Describing functions were used to relate the input and output of the nonlinear model. Because of the variability of hysteresis, the correlation between the calculated and the measured limit-cycle characteristics was considered to be good.

During a flight with a modified electronic filter, a severe vibration was encountered in which the stability augmentation system served as a feedback and caused the horizontal stabilizers to resonate. An analysis, based on the assumption that the fuselage was a rigid but free body reacting to the vibrating flexible horizontal stabilizers, explained the instability. The computed critical gains of the stability augmentation system were about one-third as large as the experimentally determined values.

An analysis was also made in which the right and left damper channels were assumed to have unequal gains in order to explain an interdependency between the roll and pitch axes evident in the experimental results.

A notch electronic filter for the stability augmentation system, which was designed to give minimum phase lag at limit-cycle frequencies and a maximum of attenuation at the natural frequencies of the structure, proved to be successful in eliminating surface resonance and alleviating the limit-cycle problem. However, small-amplitude limit cycles still persist at some flight regimes.

In view of the unsatisfactory test results with a pressure-feedback valve for the surface actuators and the success of the notch filter, the decision was made to discontinue development of the pressure-feedback valve.

The electronic filter of the stability augmentation system was redesigned so that although limit cycles of small amplitude remain, the potentially dangerous flight conditions lie outside the operating flight envelope of the X-15 airplane.

Flight Research Center,
National Aeronautics and Space Administration,
Edwards, Calif., August 15, 1967,
719-04-05-00-24.

REFERENCES

1. Taylor, Lawrence W., Jr.; and Merrick, George B.: X-15 Airplane Stability Augmentation System. NASA TN D-1157, 1962.

2. Tremant, Robert A.: Operational Experiences and Characteristics of the X-15 Flight Control System. NASA TN D-1402, 1962.

3. Row, Perry V.; and Fischel, Jack: X-15 Flight-Test Experience. Astronaut. and Aerospace Eng., vol. 1, no. 5, June 1963, pp. 25-32.

4. Grabbe, Eugene M.; Ramo, Simon; and Wooldridge, Dean E.: Handbook of Automation, Computation, and Control. Vol 1. John Wiley & Sons, Inc., 1958, pp. 25-13 - 25-36.

5. Howard, Vincent W.: The Effects of Structural Elasticity on Aircraft Control Systems. Tech. Rep. 56-166, Wright Air Dev. Center, U.S. Air Force, June 1956.

6. Mechtly, E. A.: The International System of Units - Physical Constants and Conversion Factors. NASA SP-7012, 1964.

7. Cooper, N. R.: X-15 Flight Simulation Program. Aerospace Eng., vol. 20, no. 11, Nov. 1961, pp. 16, 17, 71-77.

8. Deazley, William R.: A Study of Two Proposed Stabilization Techniques for the X-15 Horizontal Surface Control System. Rep. No. TB-1568-F-1, Cornell Aero. Lab., Inc., Aug. 10, 1961.

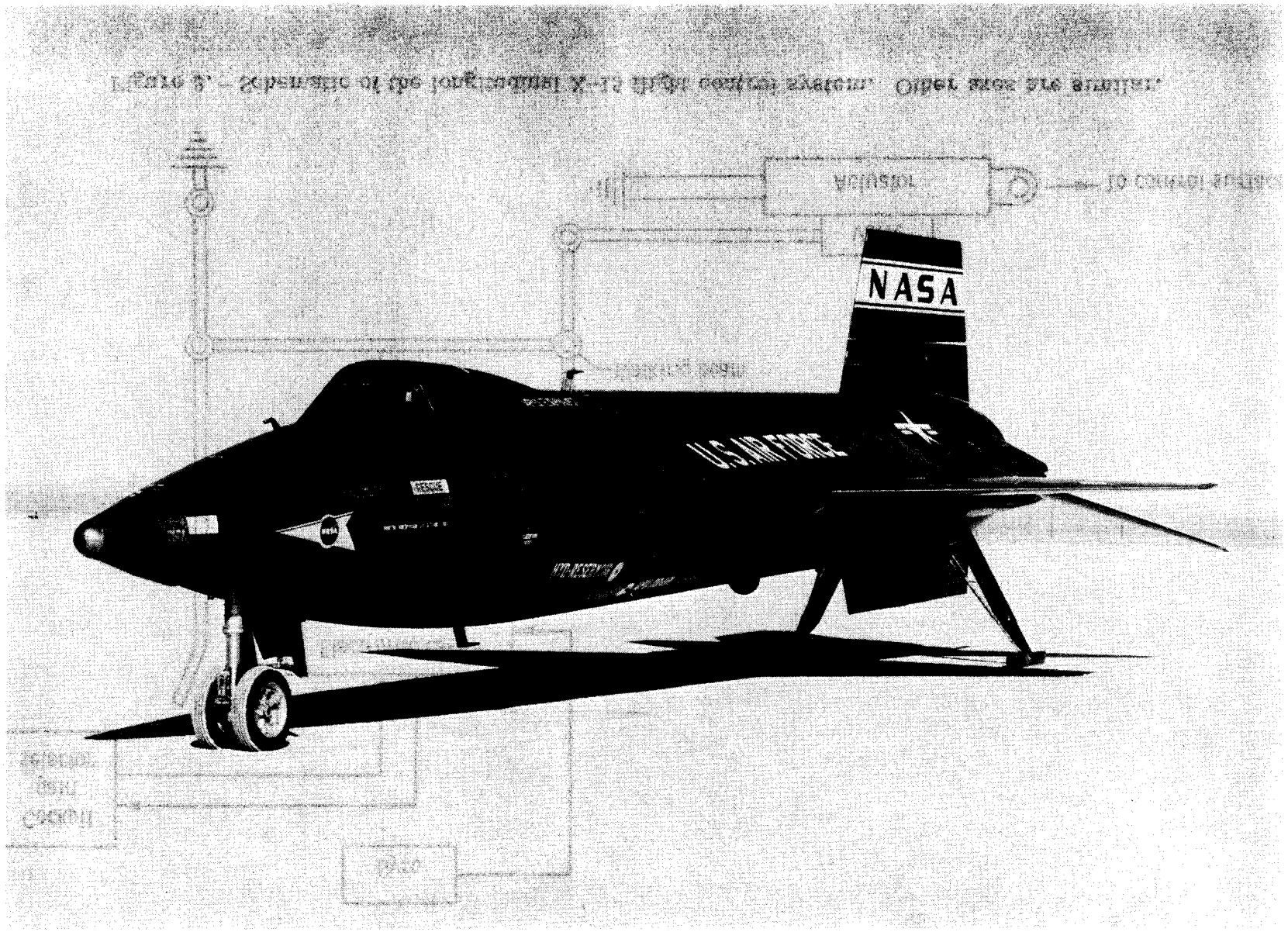

Figure 1. – X-15 airplane. E-7902

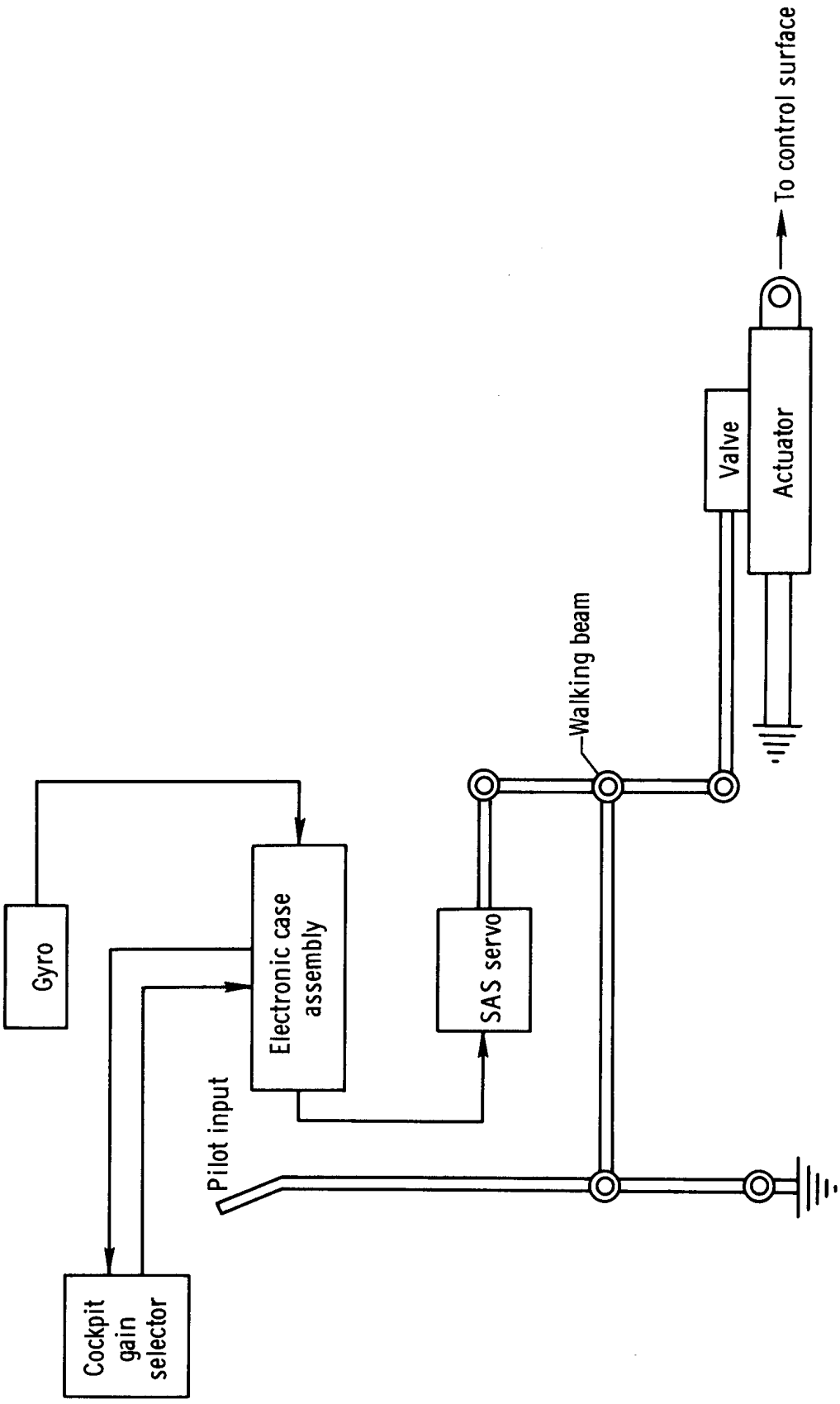

Figure 2. – Schematic of the longitudinal X-15 flight control system. Other axes are similar.

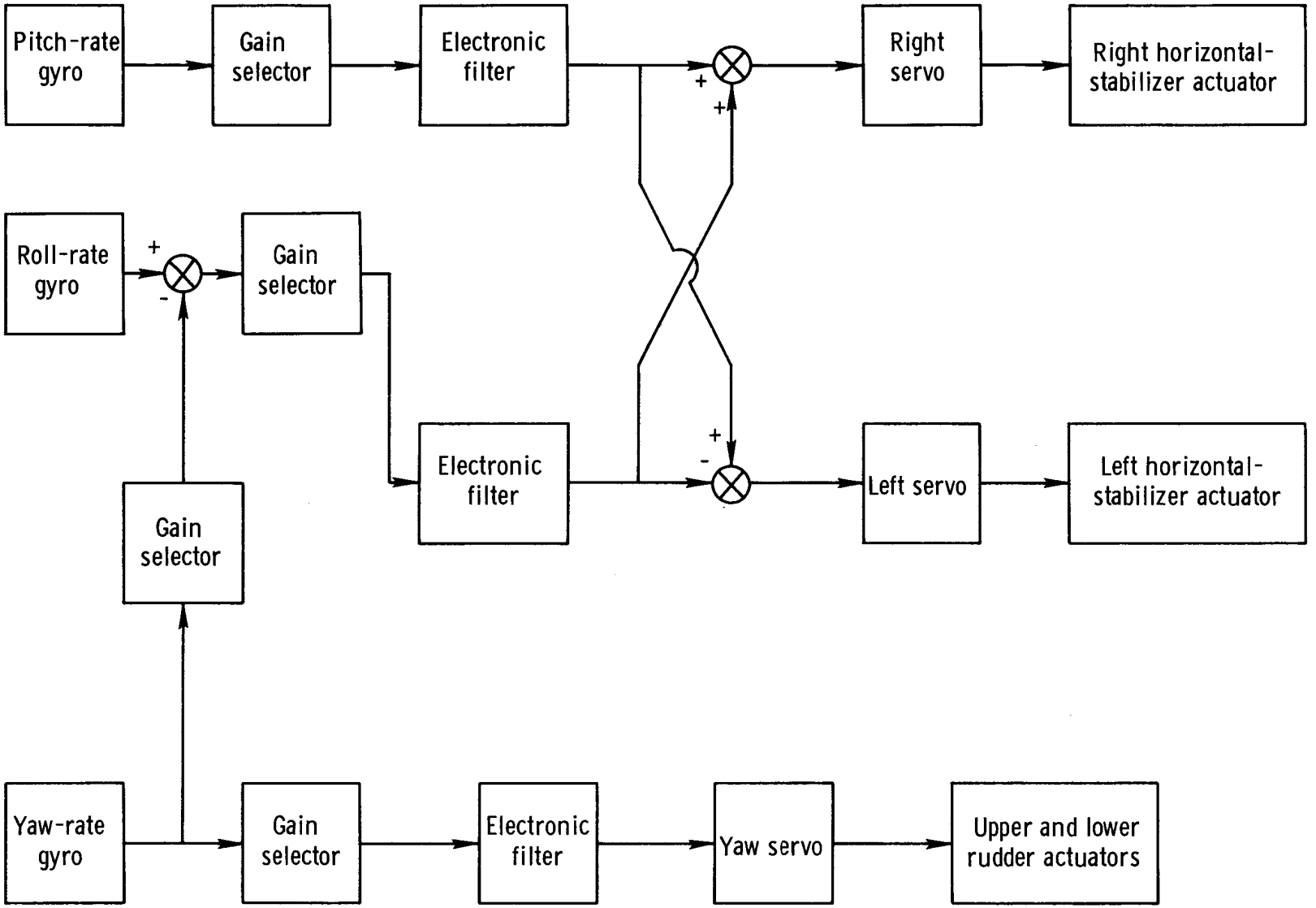

Figure 3. – Functional diagram of the stability augmentation system.

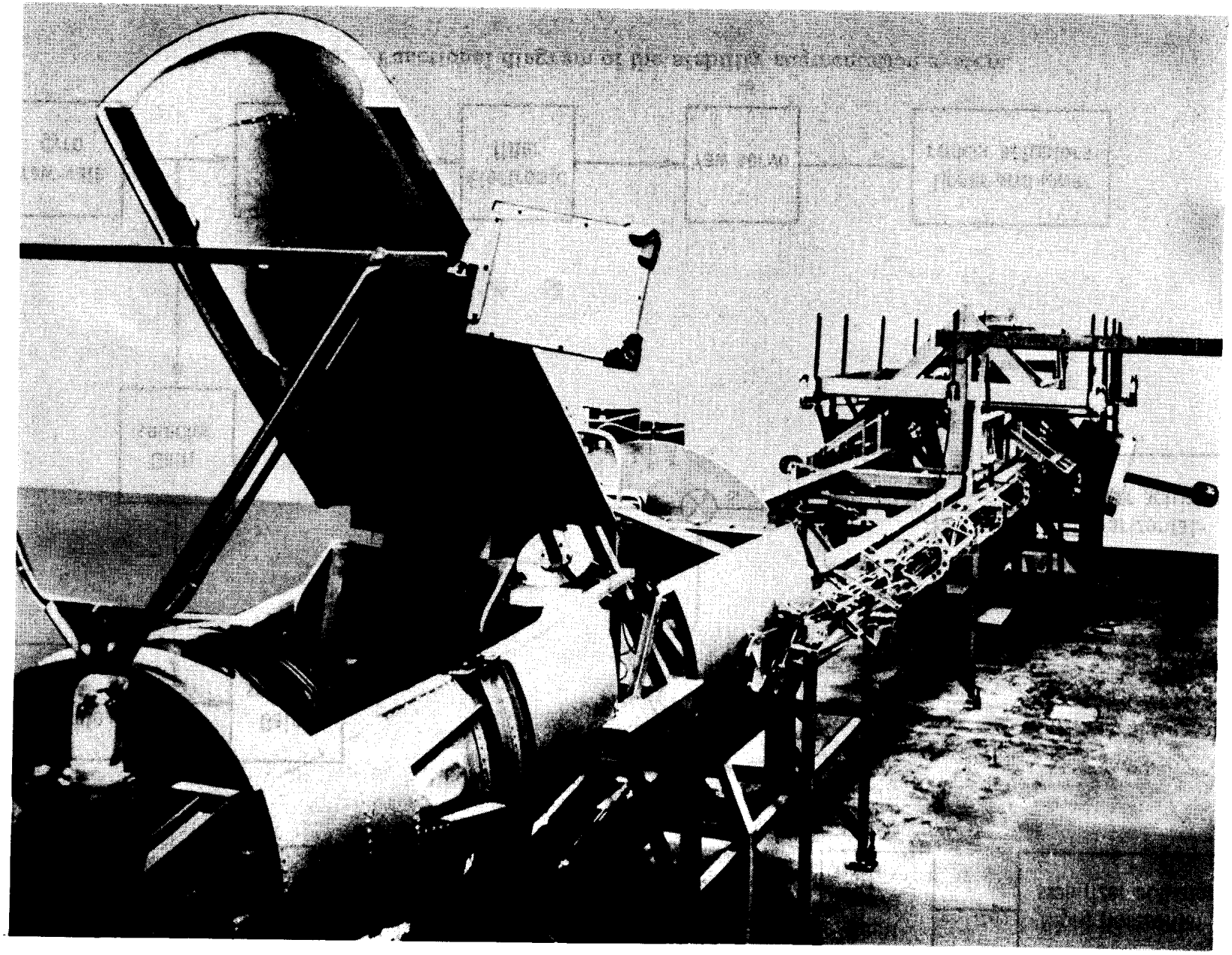

Figure 4. – X-15 flight simulator. E-6737

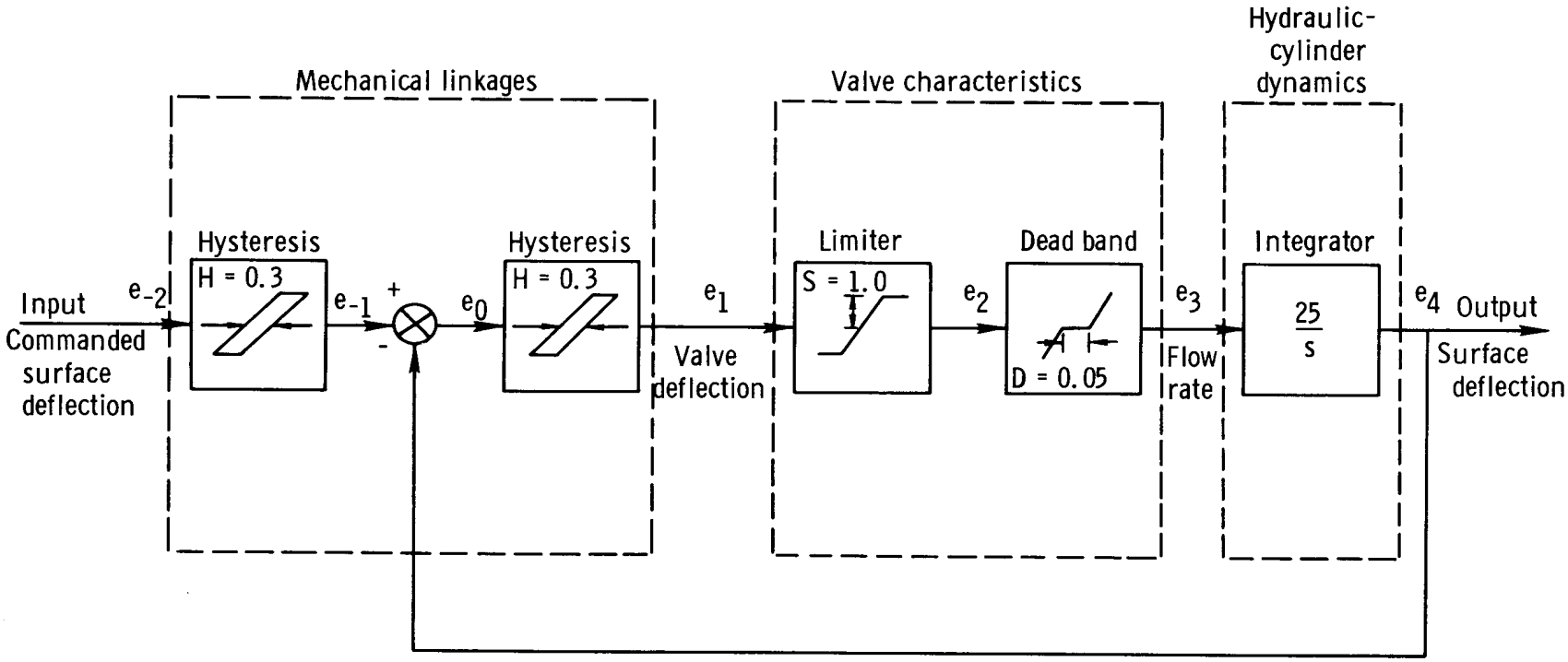

Figure 5. – Mathematical model used to describe nonlinear characteristics of the surface actuators. Gains of all nonlinear elements equal unity.

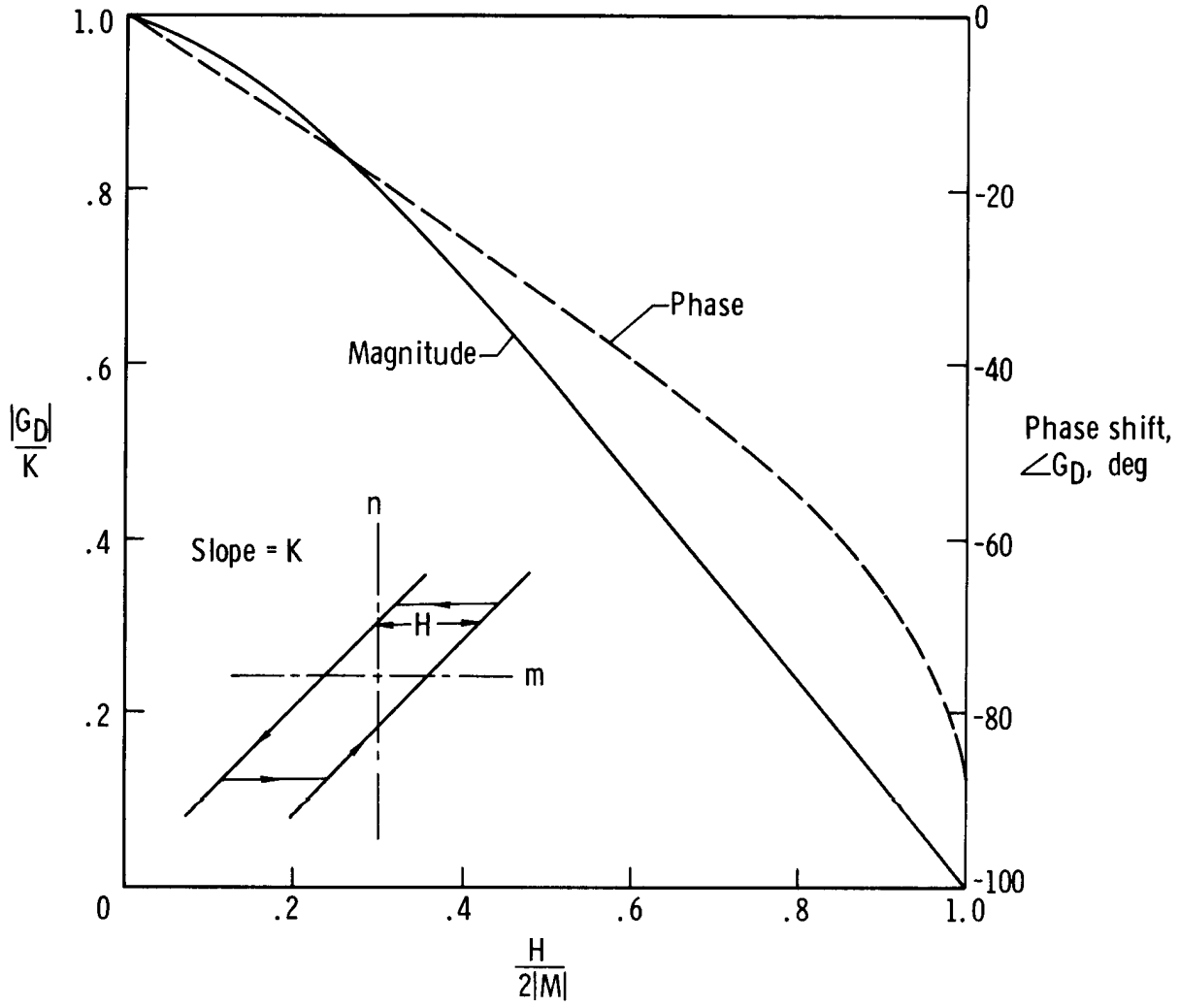

(a) Hysteresis (forward).

Figure 6. – Describing functions, based on reference 4.

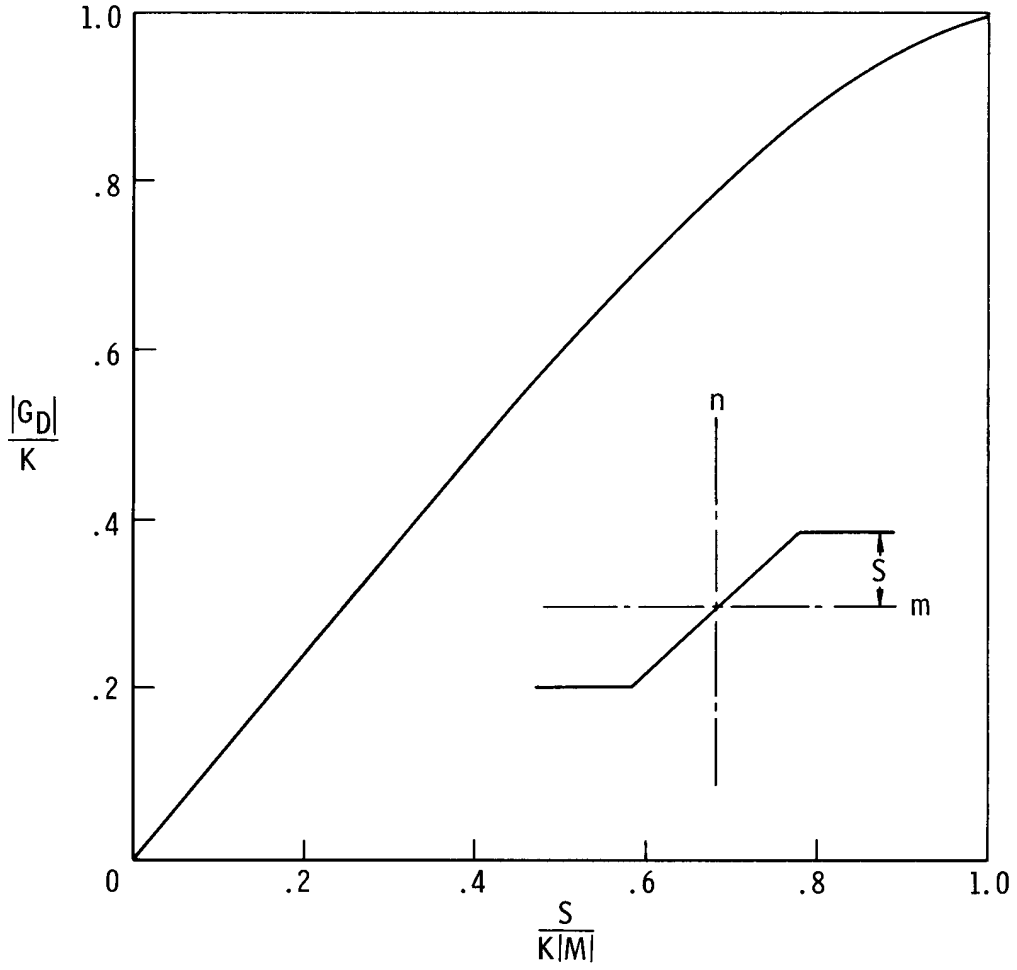

(b) Saturation.

Figure 6. – Continued.

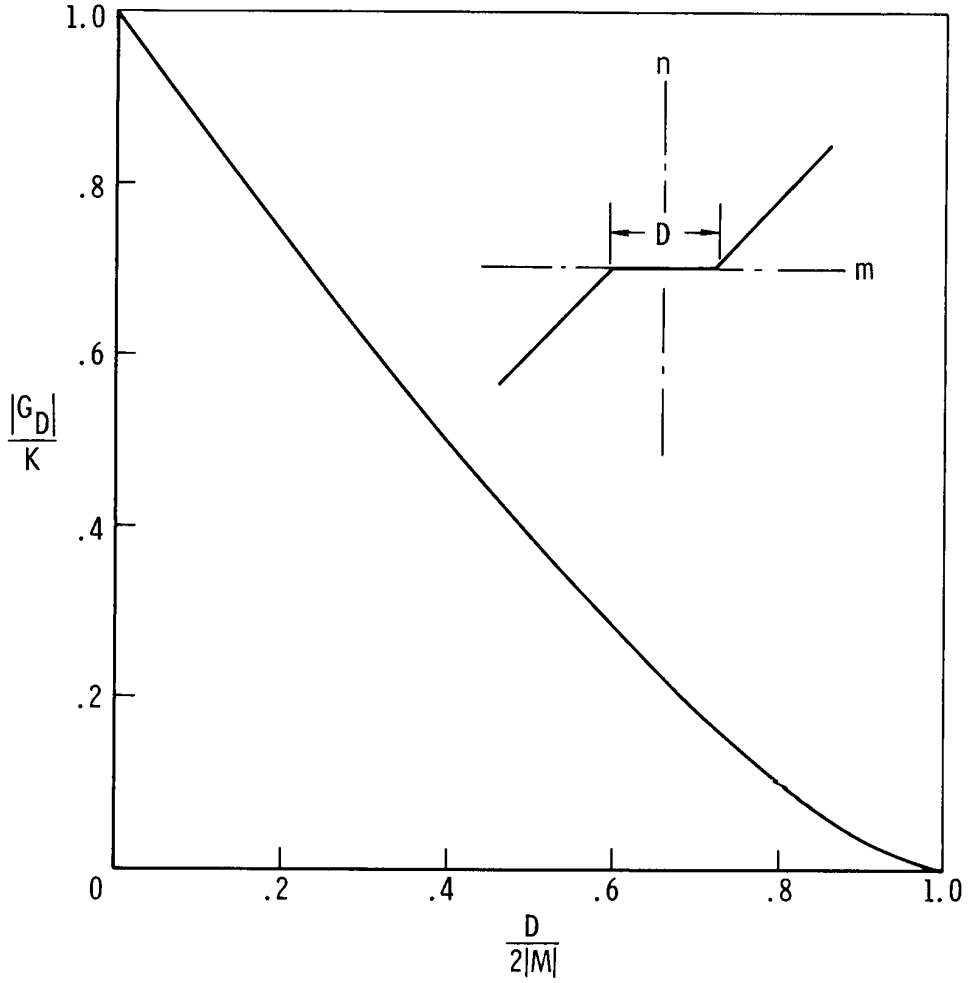

(c) Dead band.

Figure 6. – Continued.

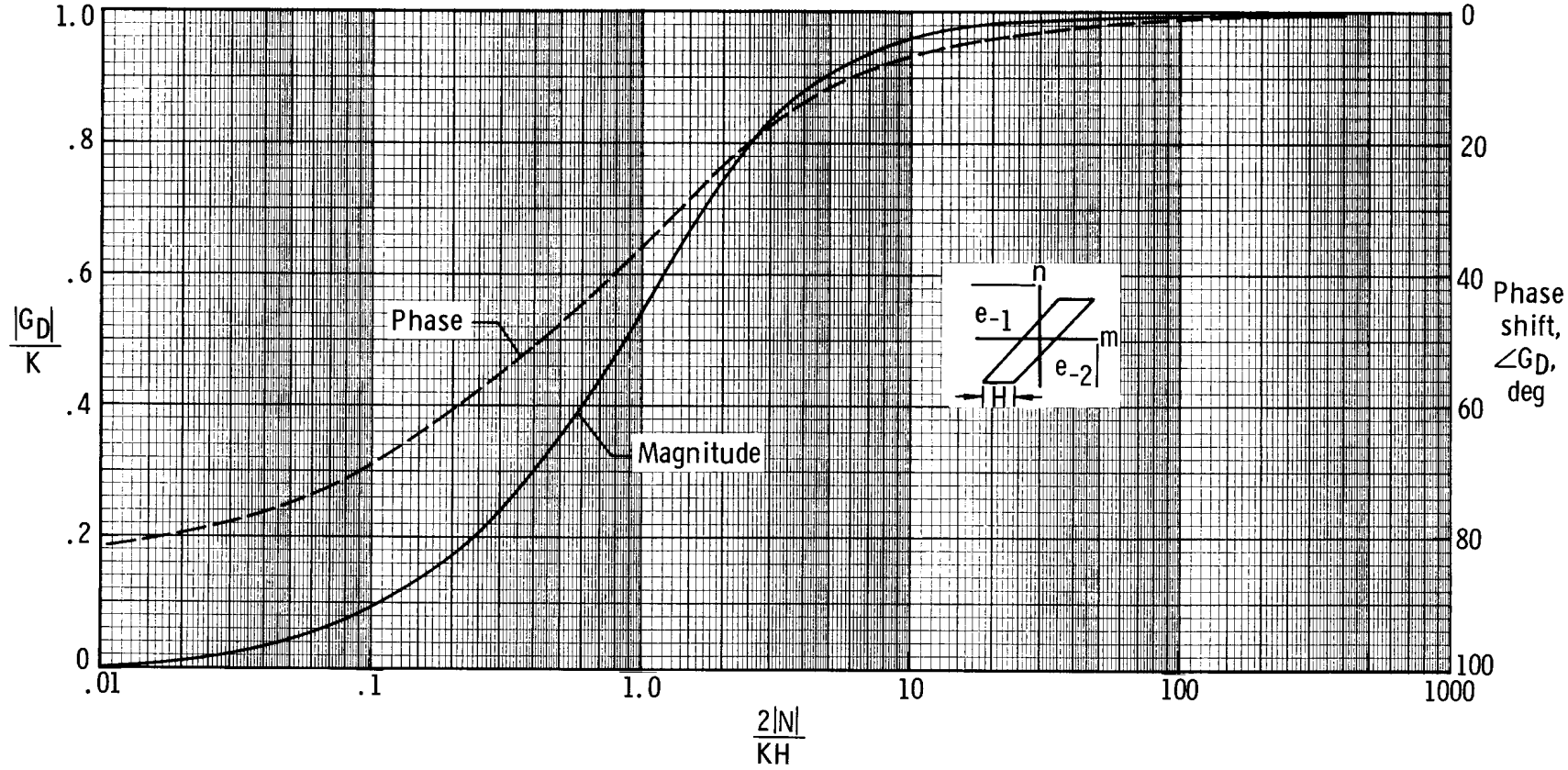

(d) Hysteresis (inverse).

Figure 6. – Concluded.

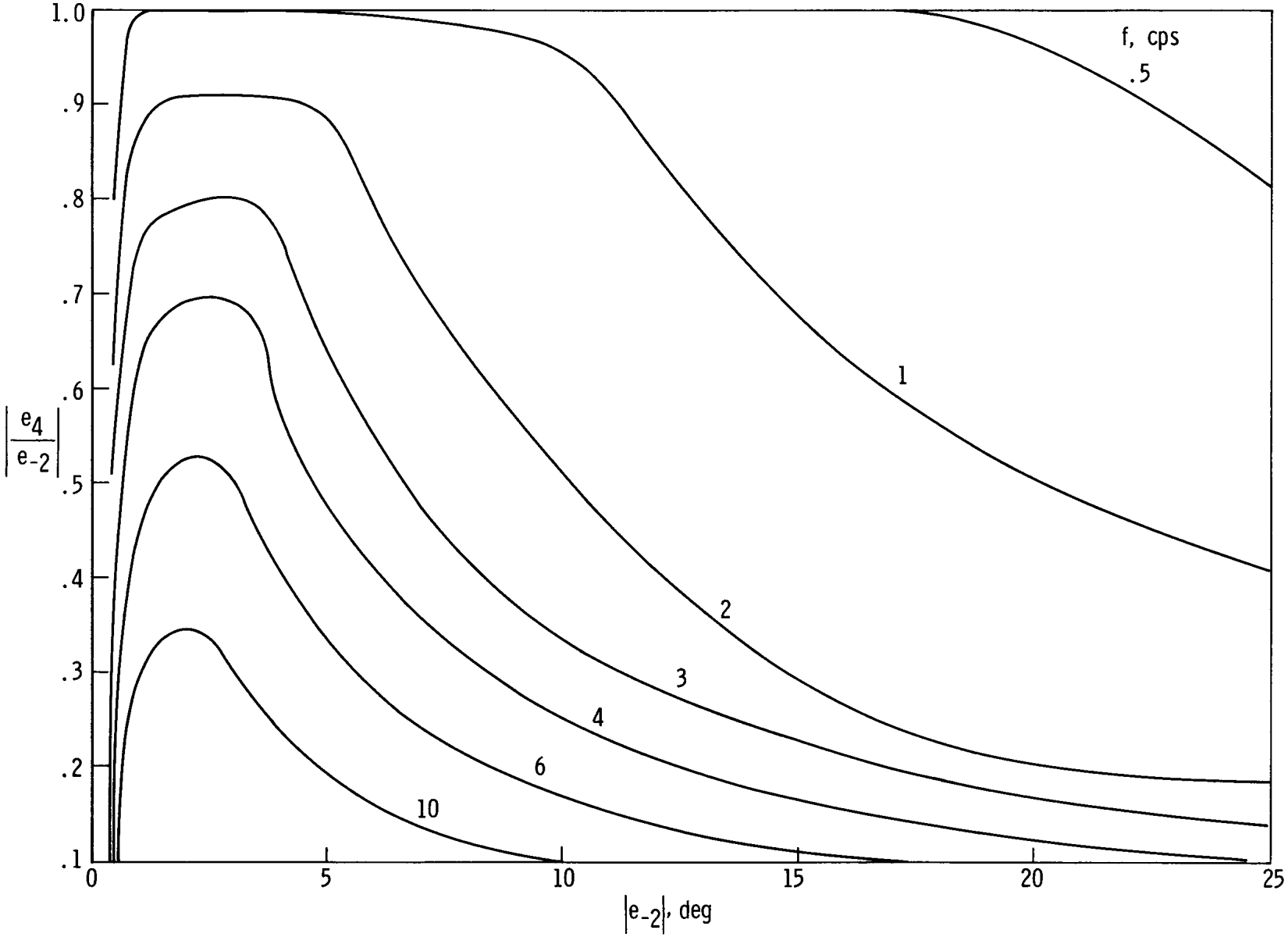

(a) Amplitude ratio.

Figure 7. – Calculated characteristics of the nonlinear portion of the control system.

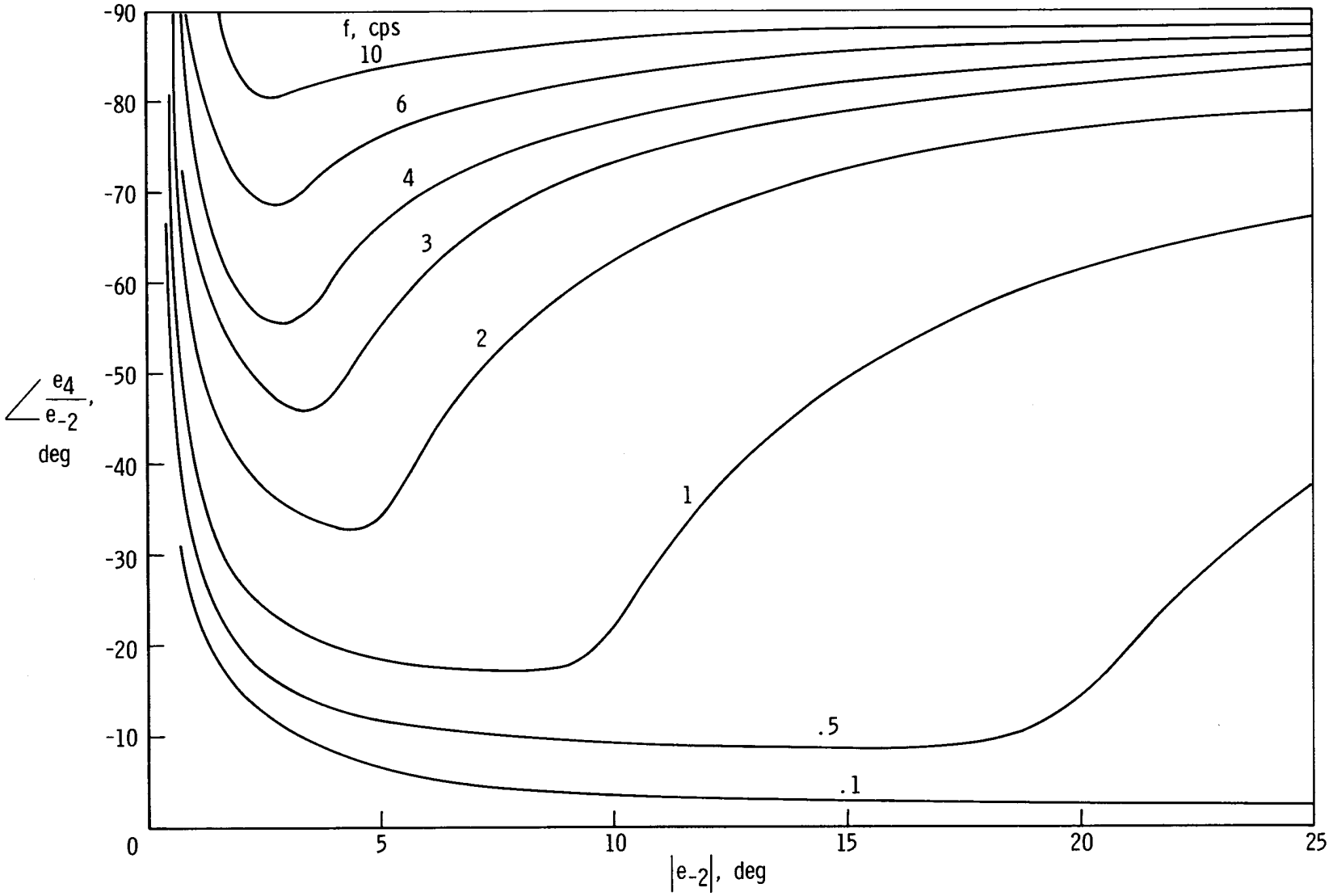

(b) Phase angle.

Figure 7. – Concluded.

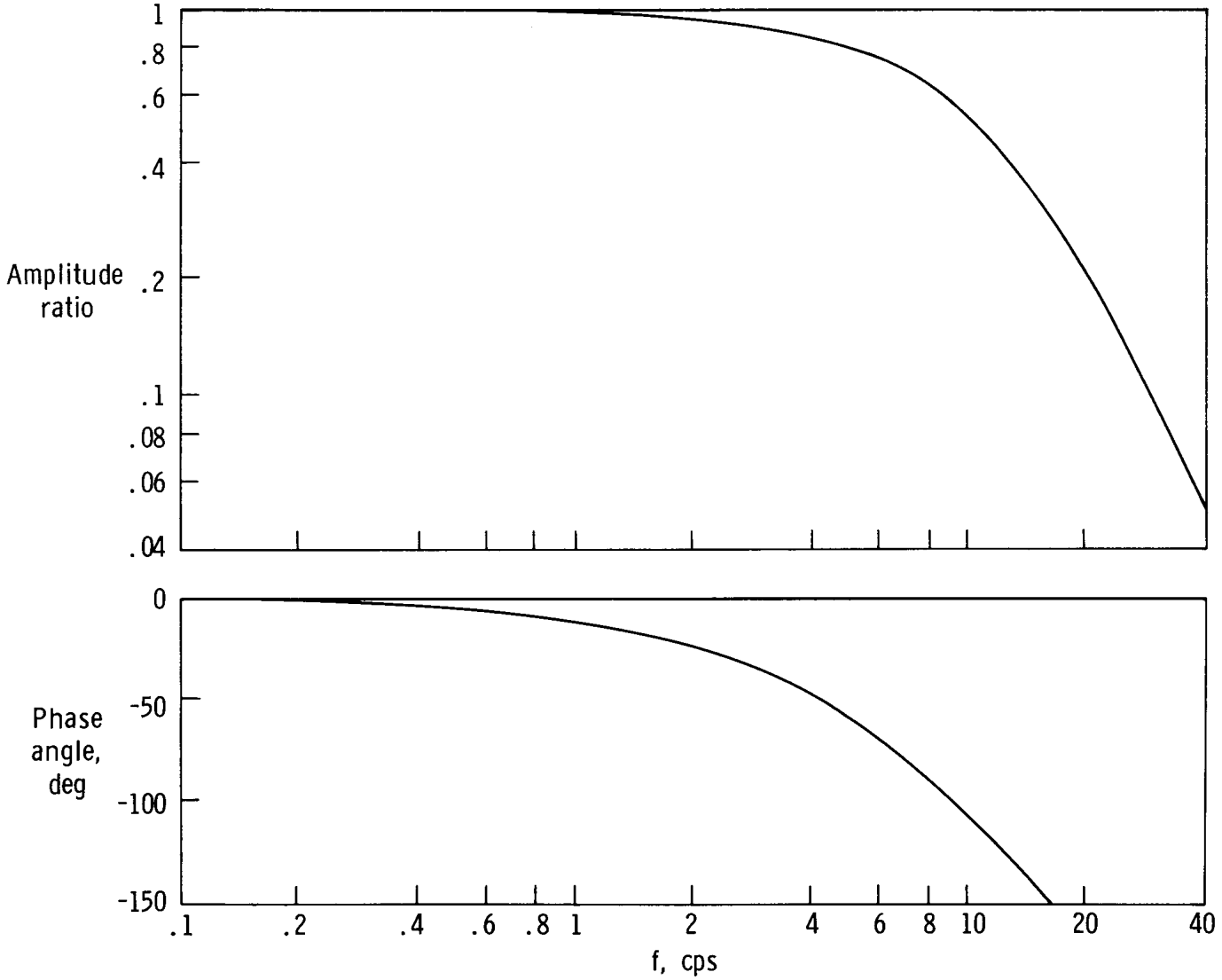

Figure 8. – Frequency response of the original electronic filter and SAS servo.

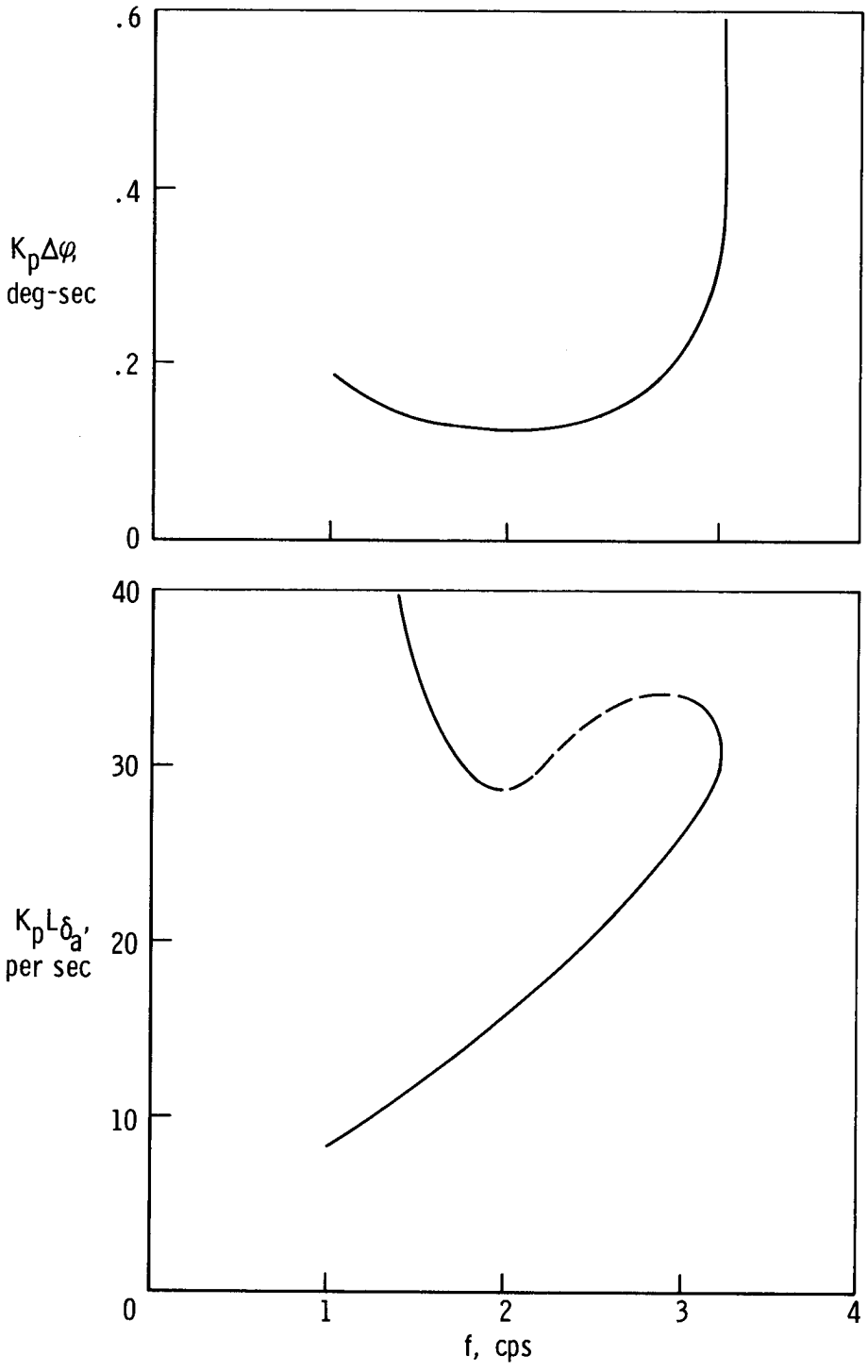

Figure 9. – Calculated roll limit-cycle characteristics for the original filter.

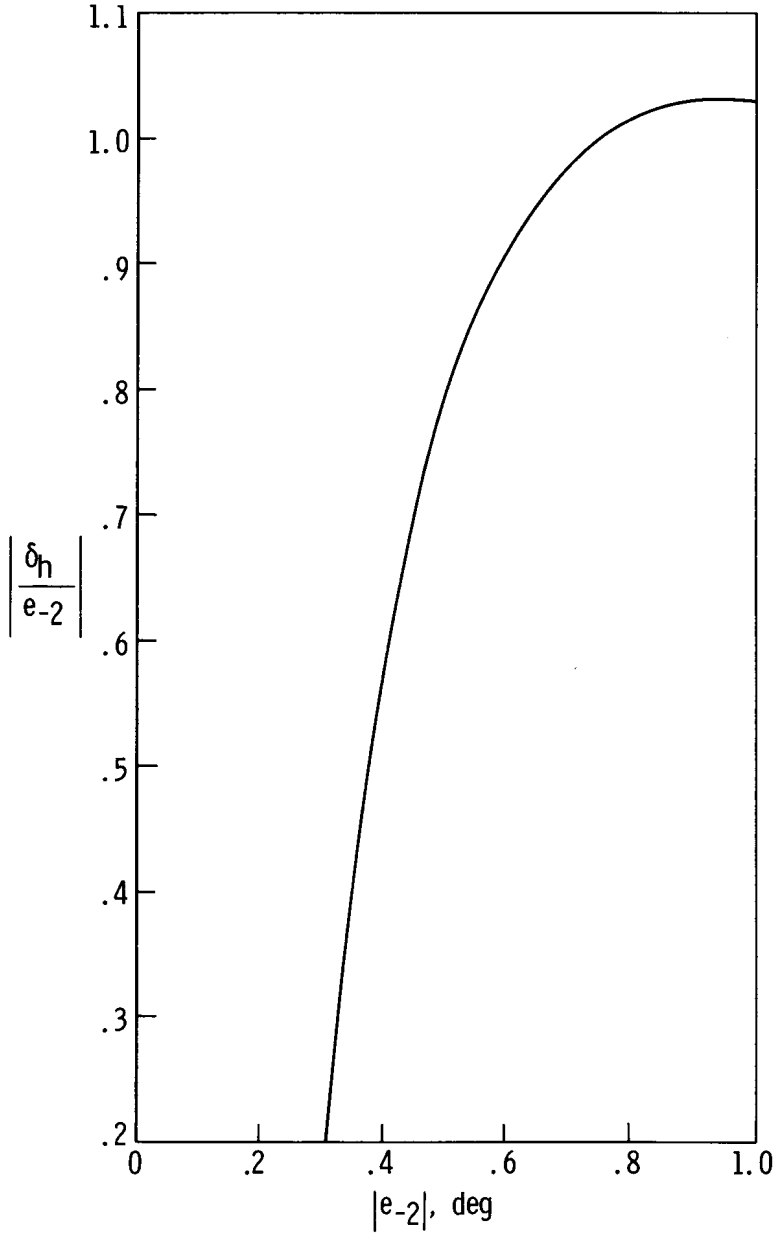

(a) Amplitude ratio.

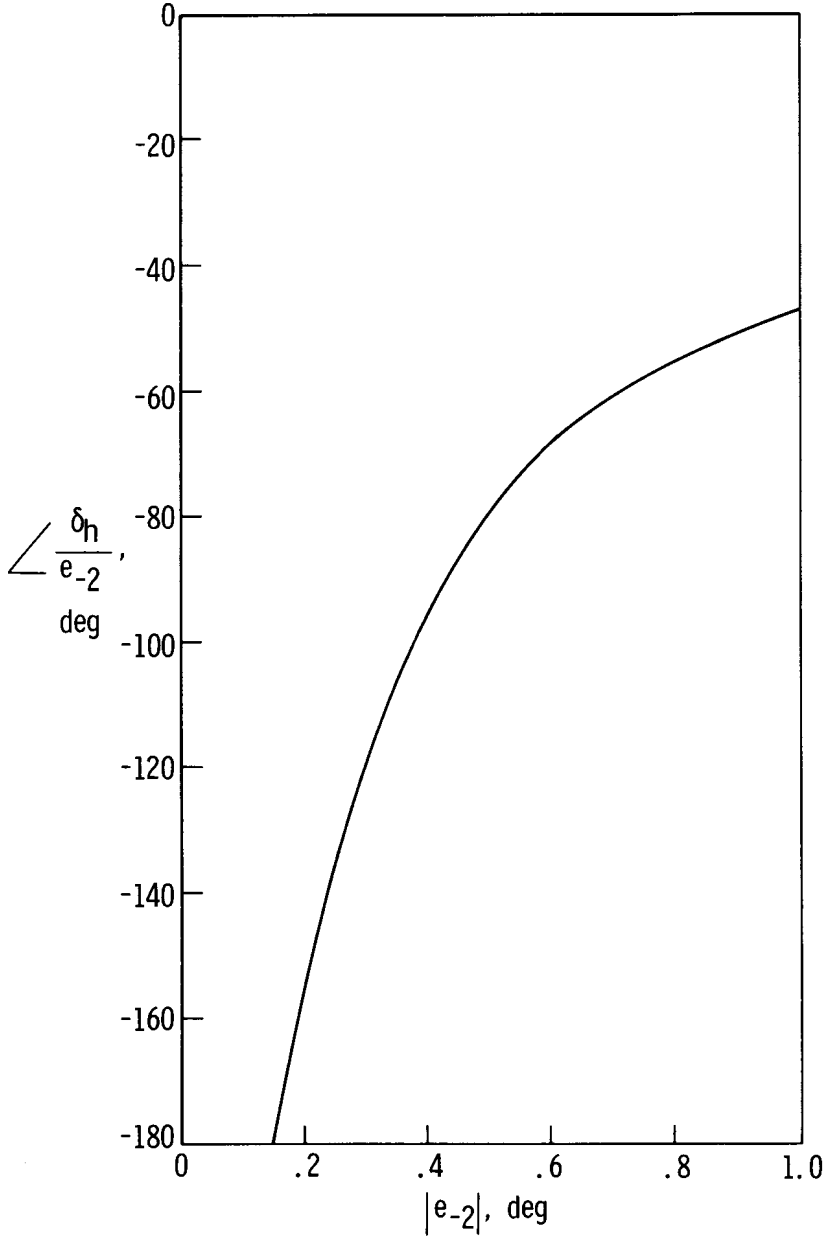

(b) Phase angle.

Figure 10. – Characteristics of the nonlinearity for pitch and yaw limit-cycle calculations.

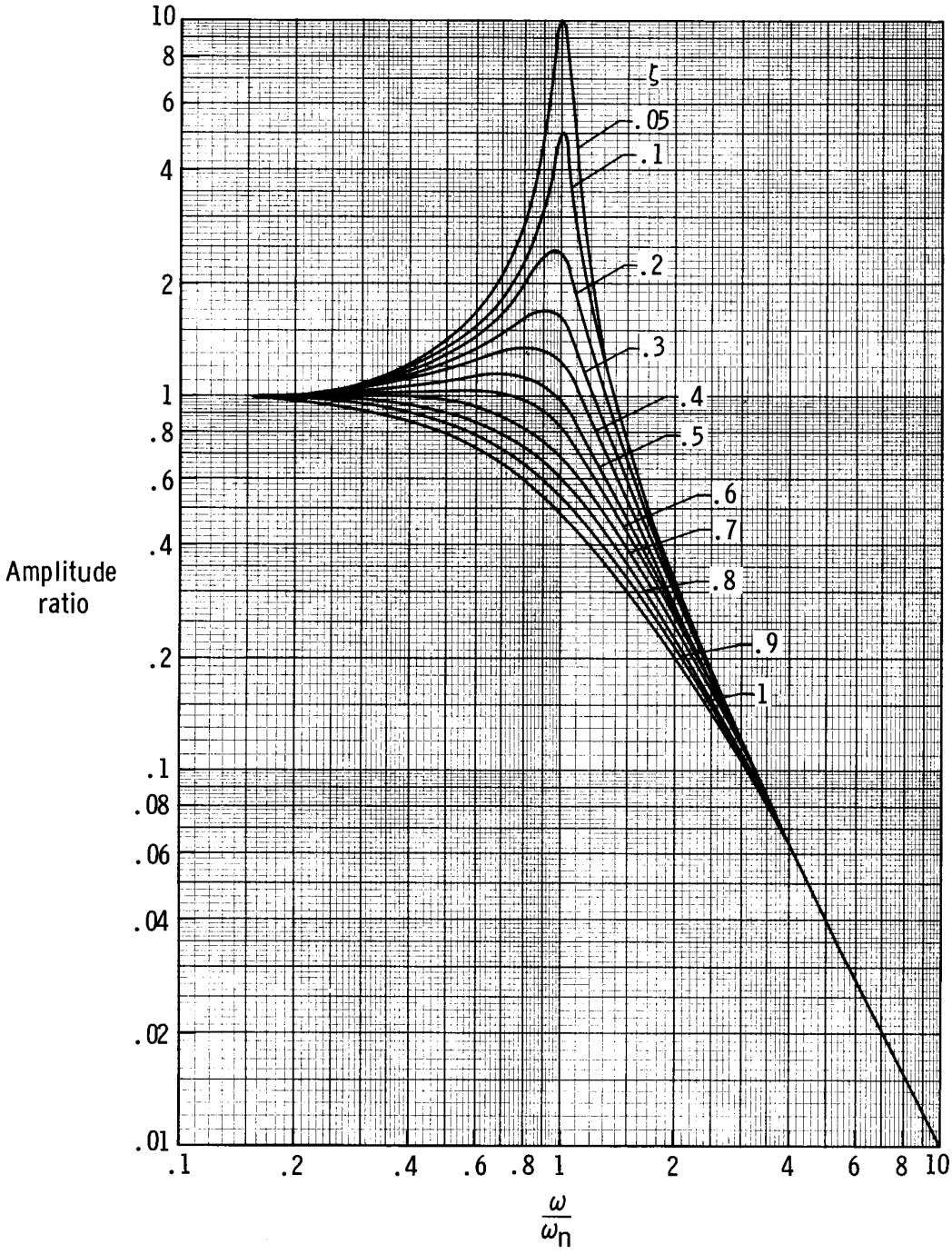

(a) Amplitude ratio.

Figure 11. – Second-order frequency response of amplitude and phase angle of the airplane transfer function in pitch and yaw used in calculating limit-cycle characteristics.

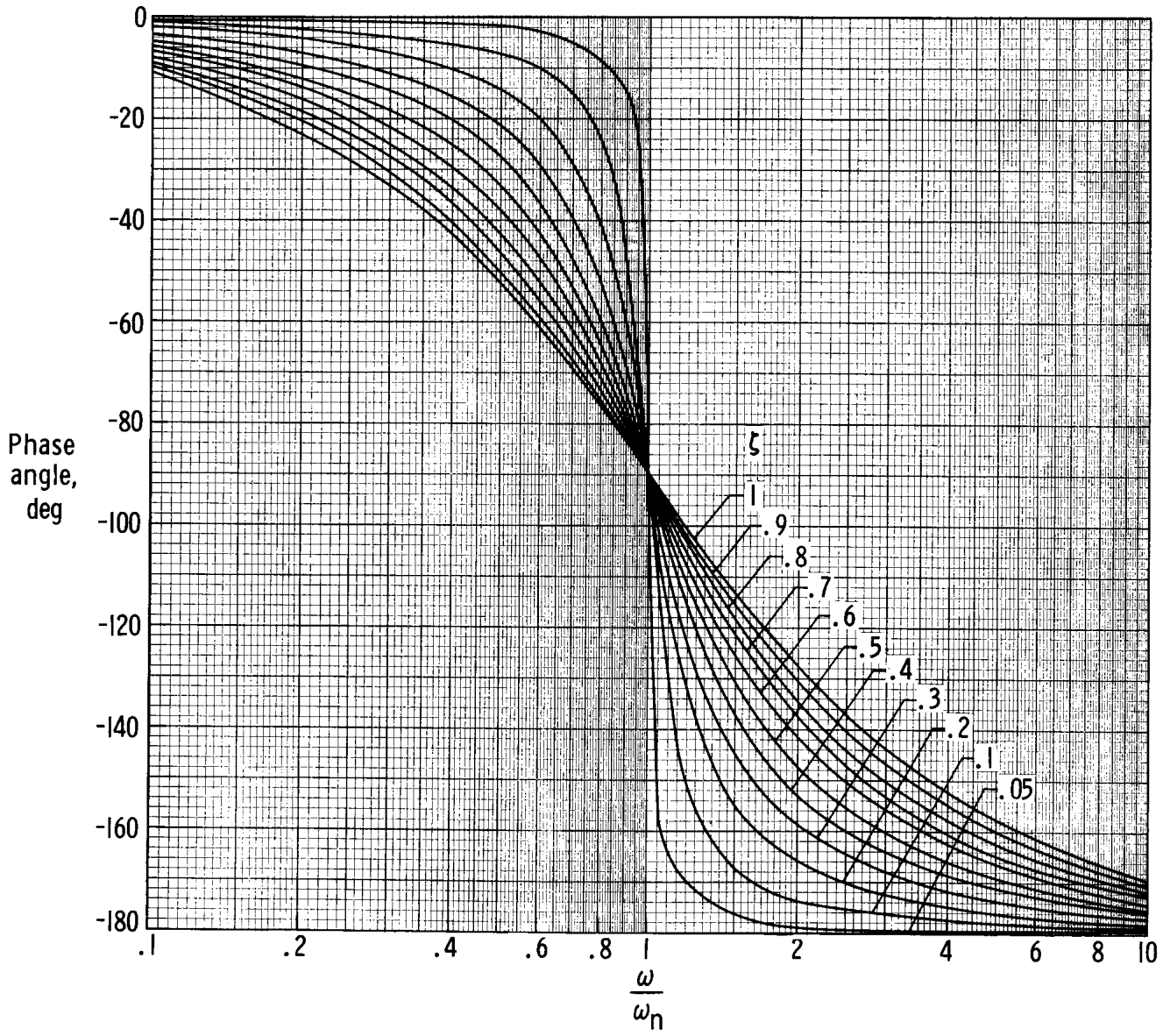

(b) Phase angle.

Figure 11. – Concluded.

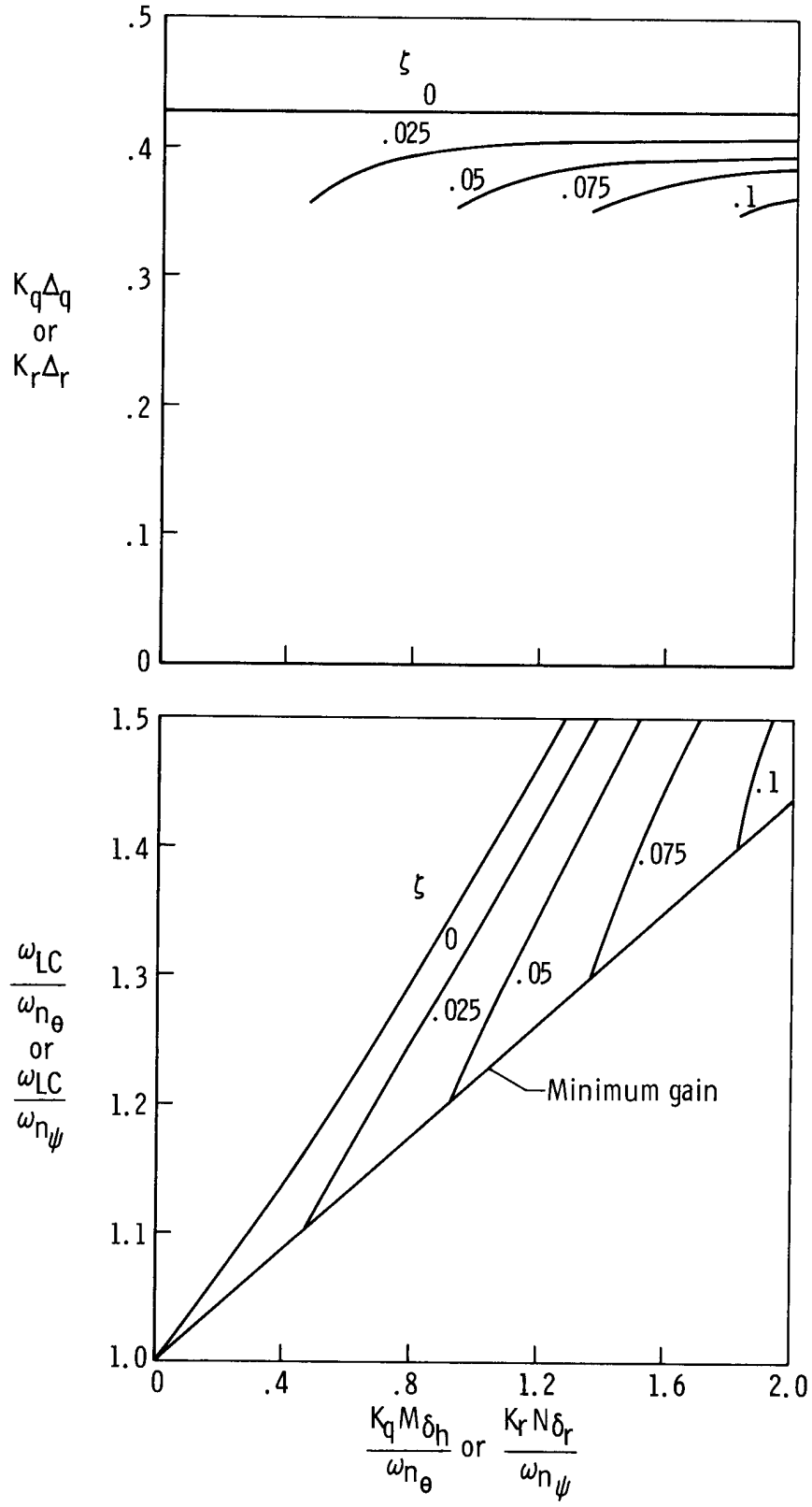

Figure 12. – Calculated pitch and yaw limit cycle characteristics.

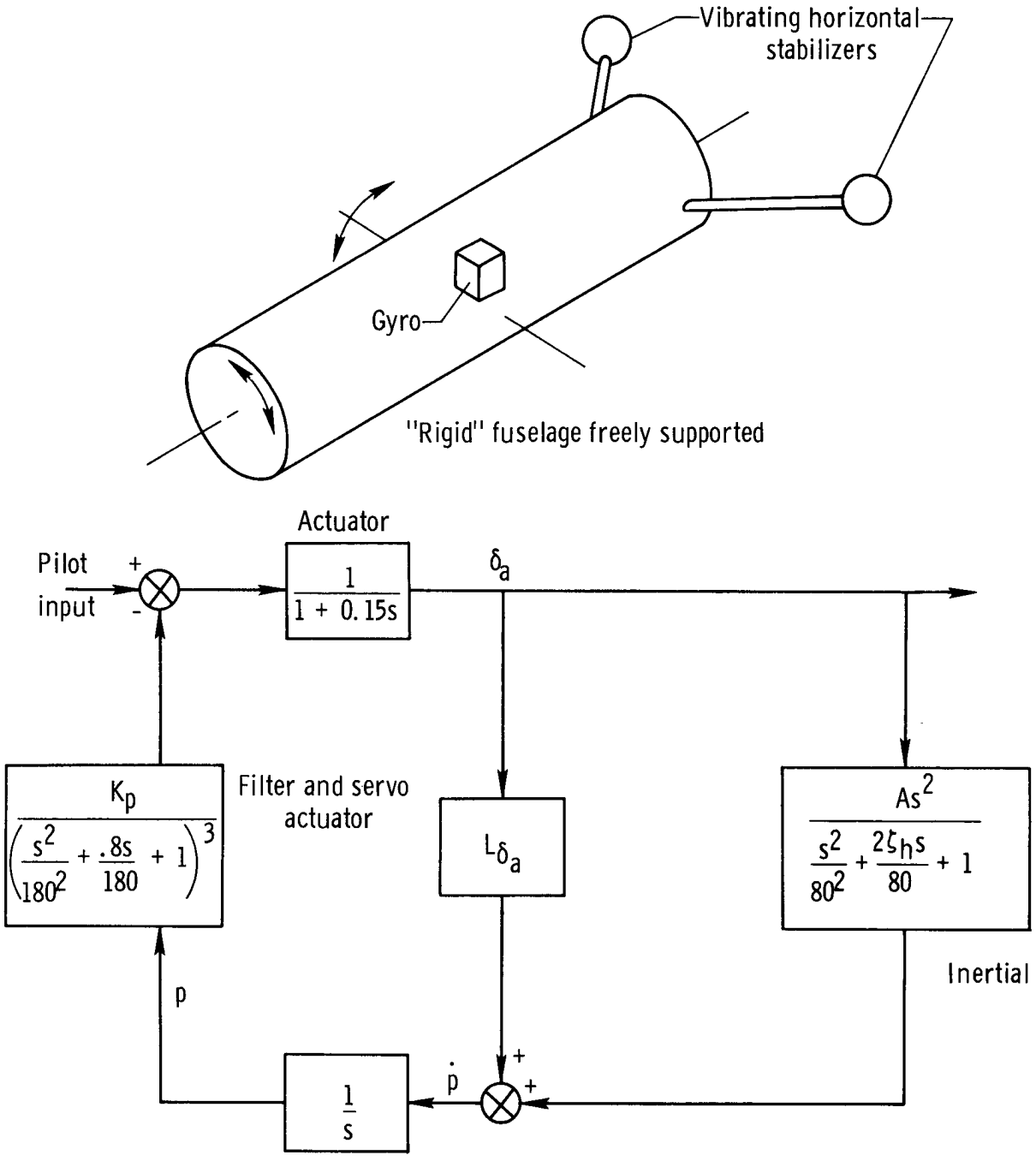

Figure 13. – Diagram of inertial and aerodynamic feedback loop.

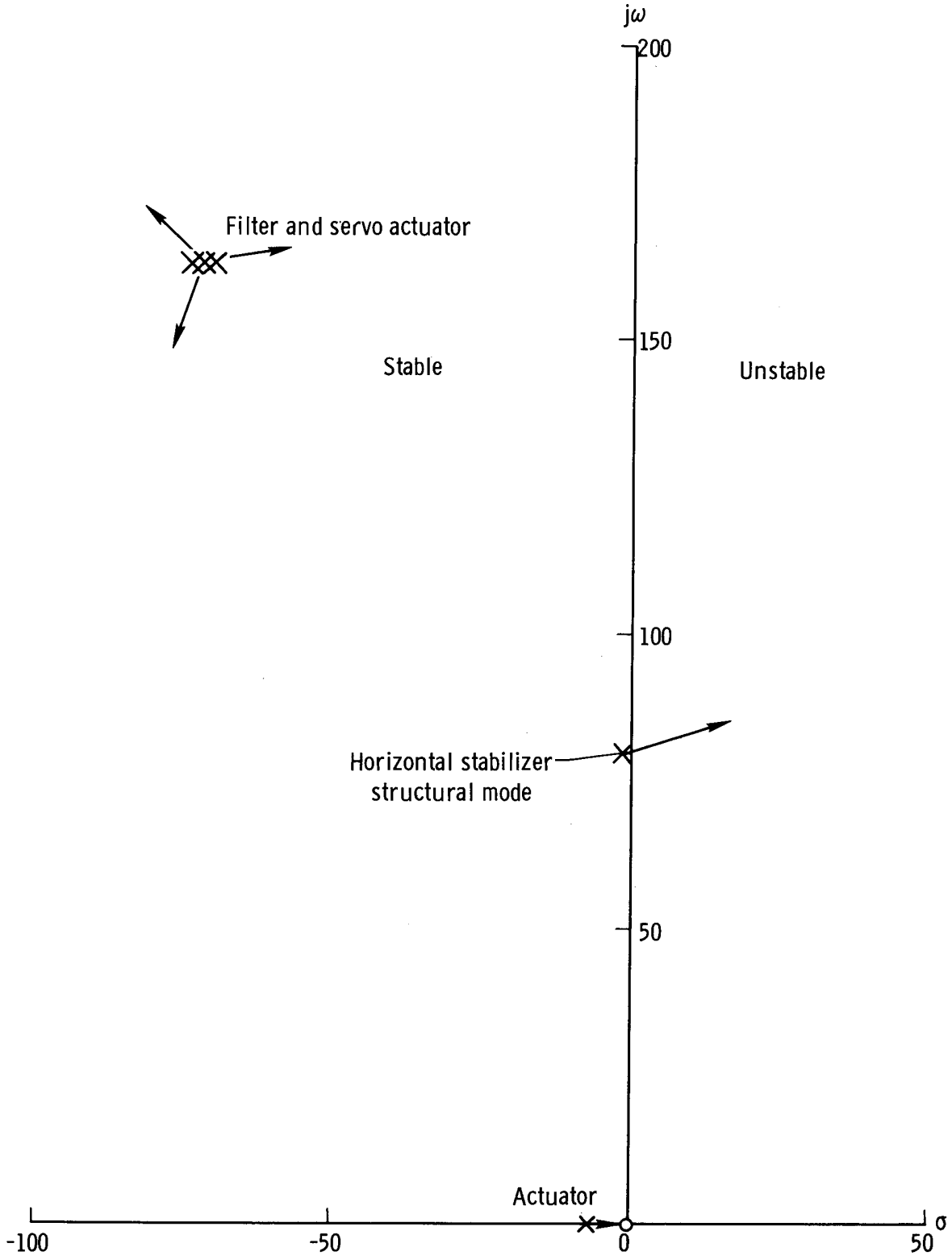

Figure 14. – Effect of inertial feedback loop on system stability.

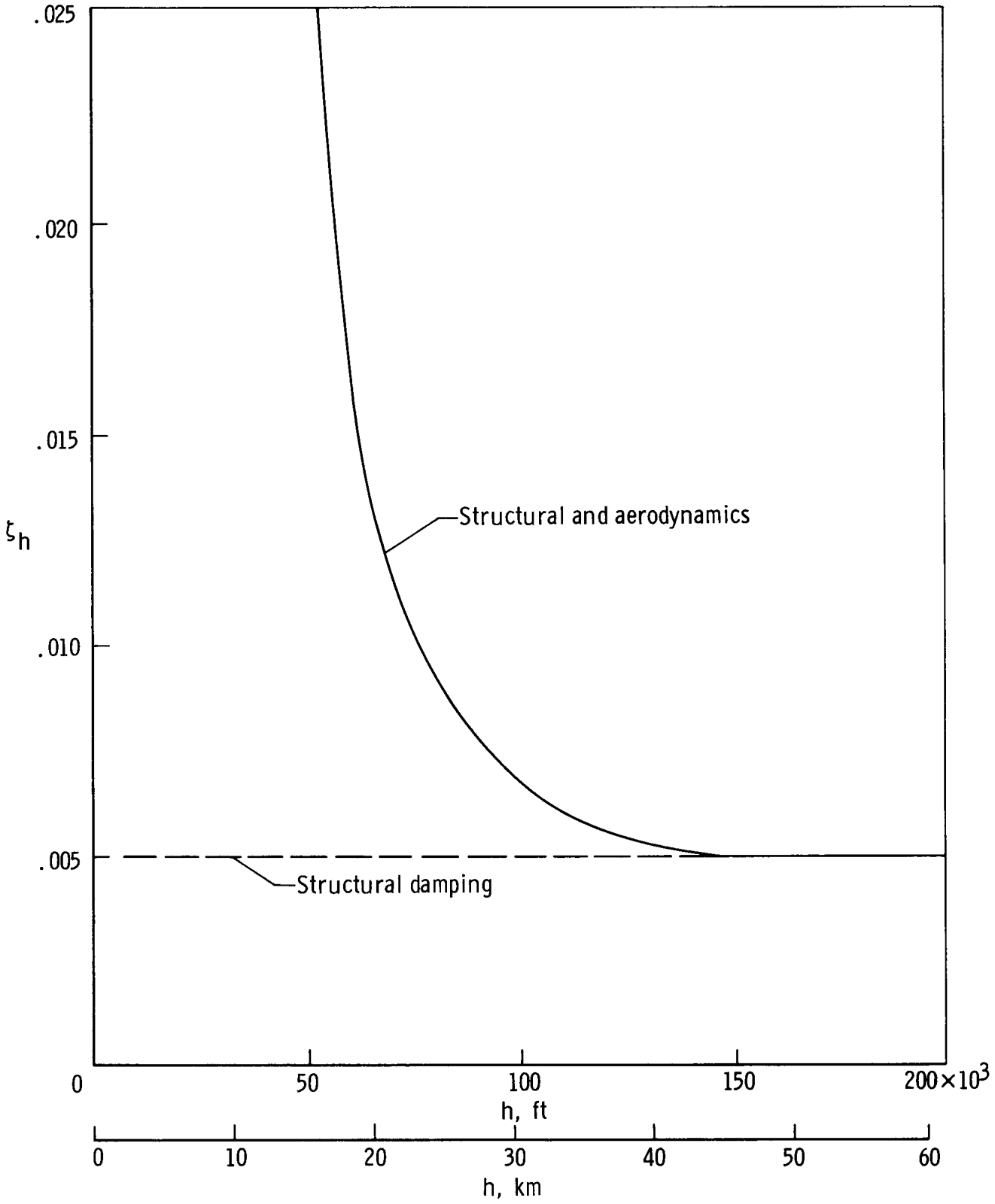

Figure 15. – Estimated horizontal-stabilizer damping as a function of altitude. Mach number > 2.

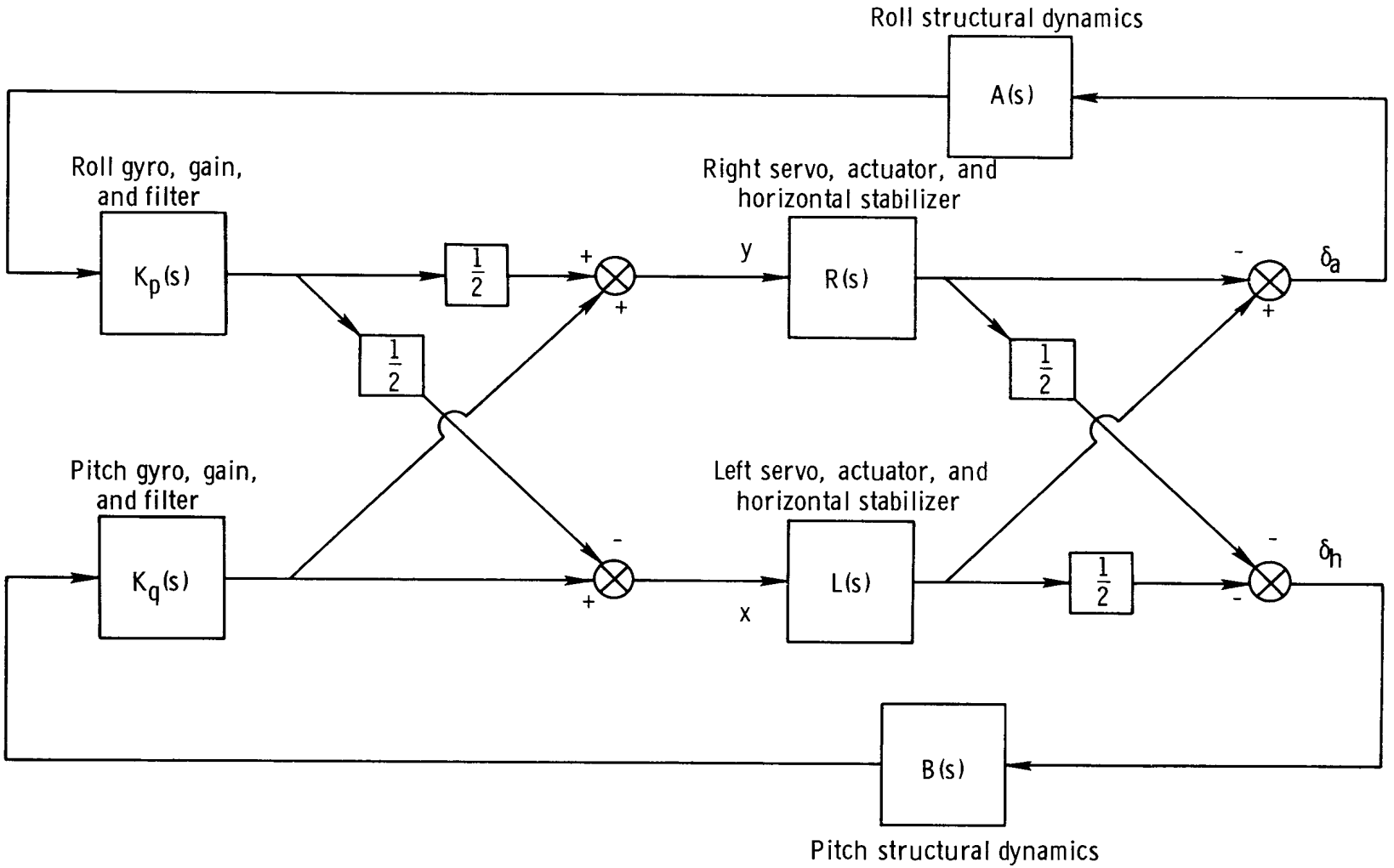

Figure 16. – Block diagram of pitch and roll inertial feedback loops.

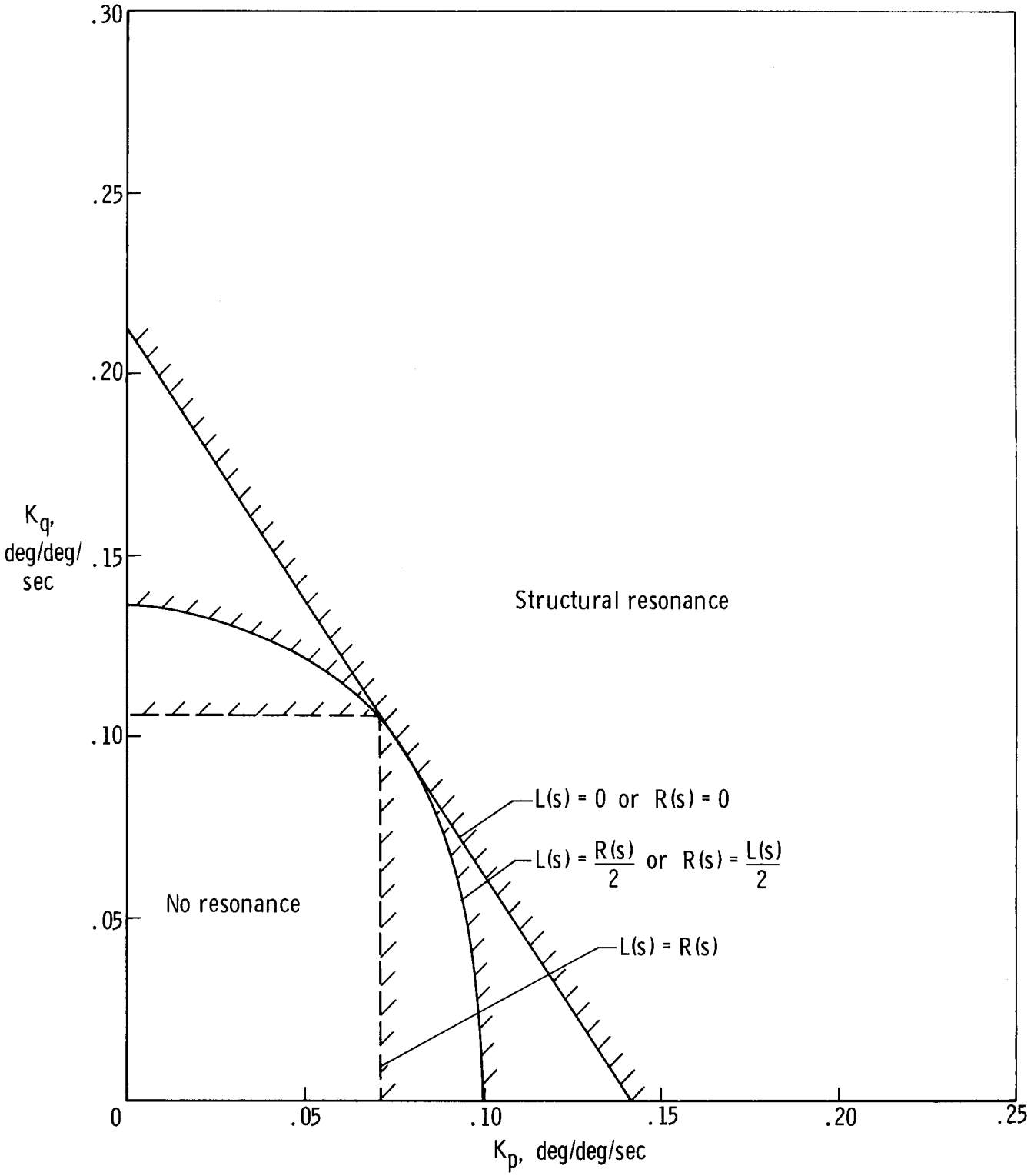

Figure 17. – Structural-resonance boundaries as a function of pitch and roll gains.

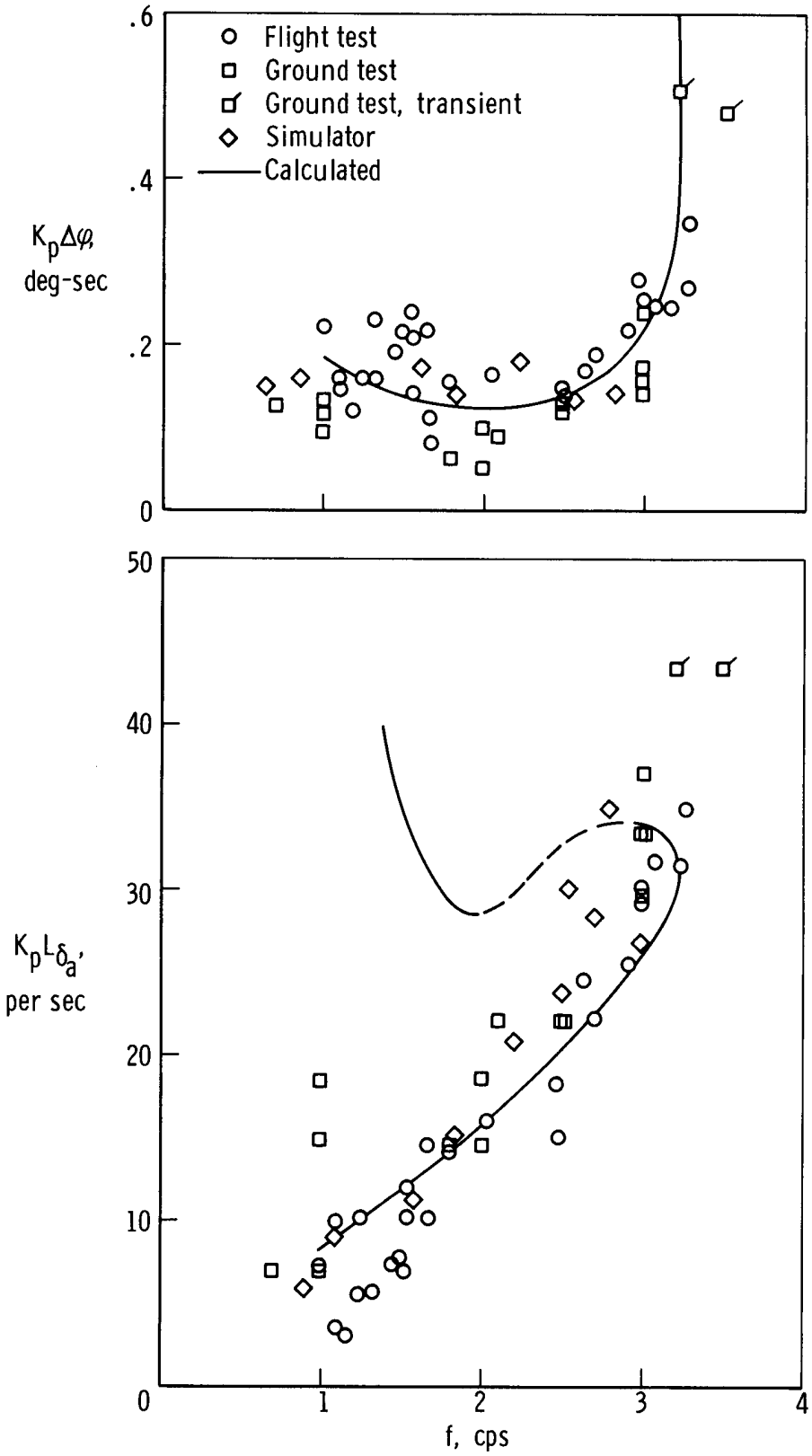

Figure 18. – Comparison of calculated and measured roll limit-cycle characteristics for the original filter.

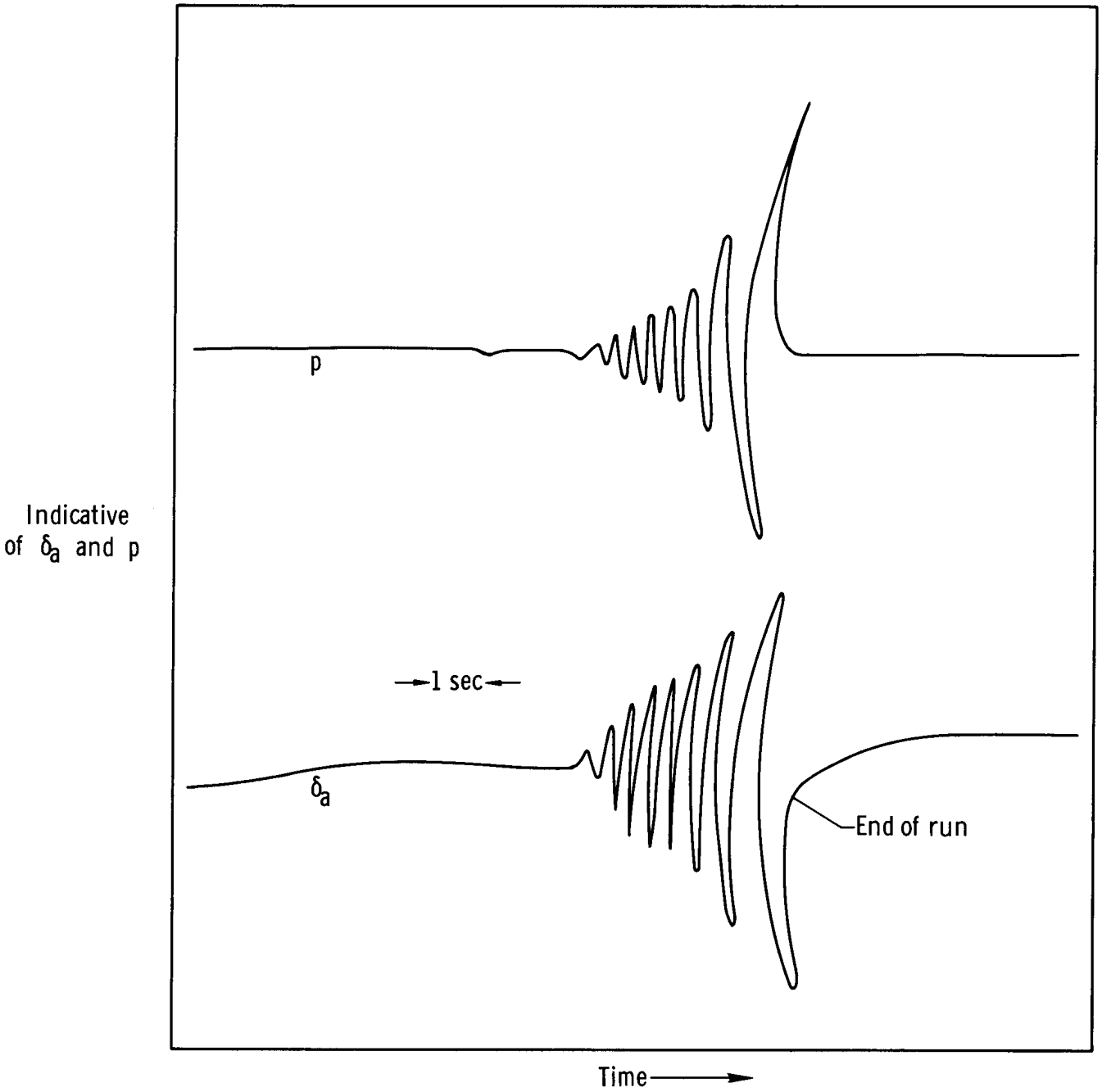

Figure 19. – Simulator time history of the transient in going to a limit cycle which corresponds to an effective gain beyond the critical value. $K_p L_{\delta_a} = 40$ per sec.

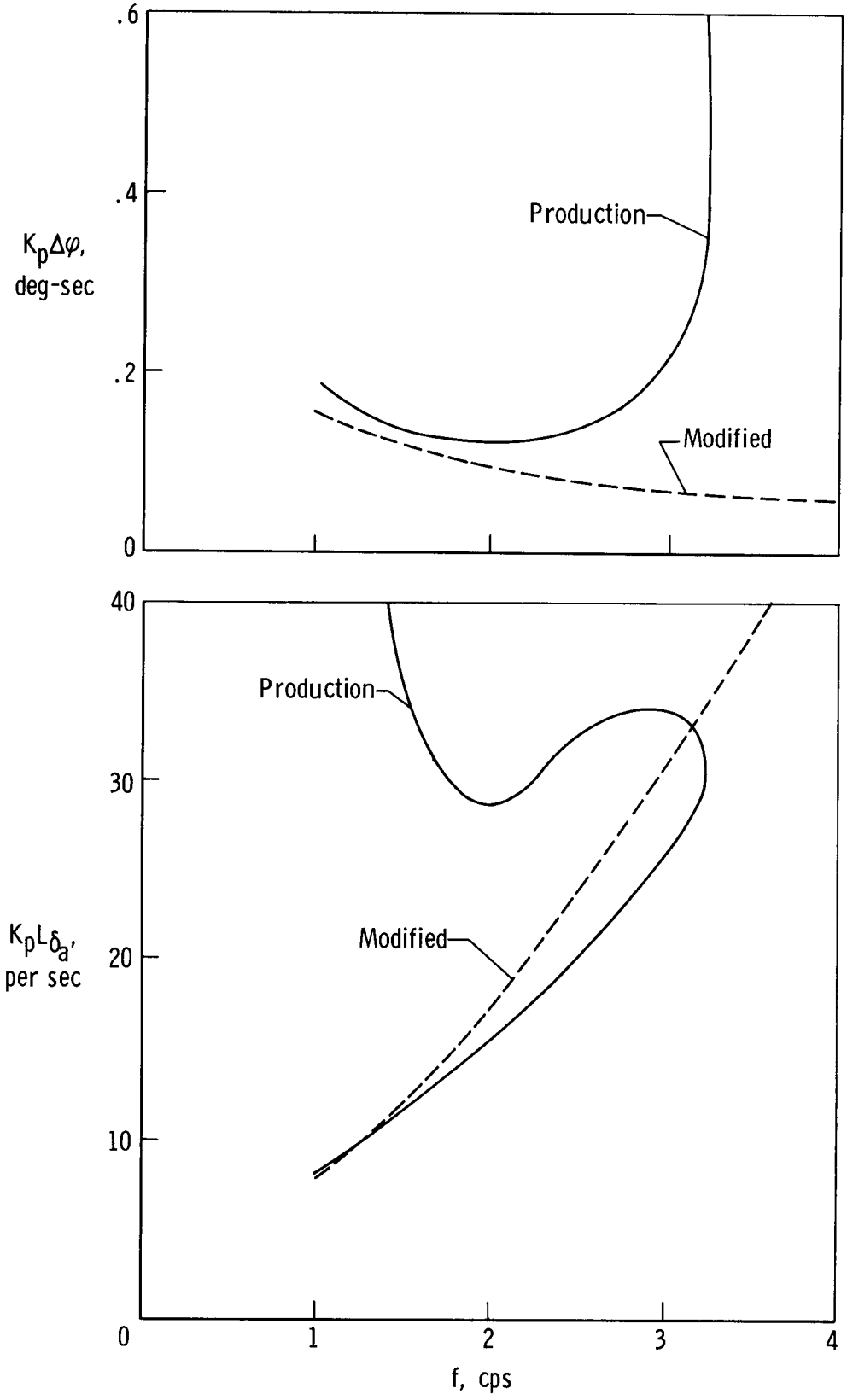

Figure 20. – Comparison of roll limit-cycle characteristics calculated for the original and the modified filters.

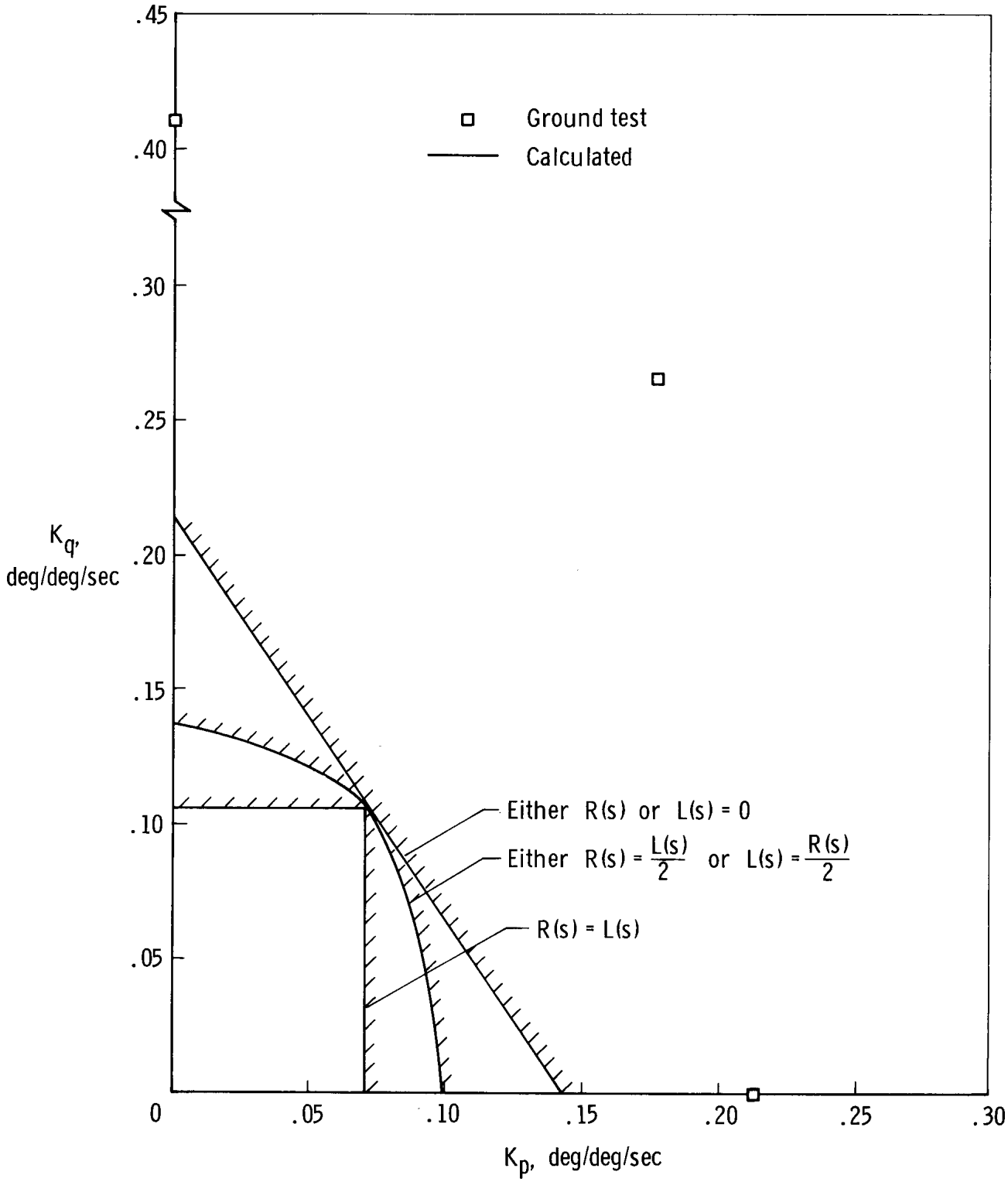

Figure 21. – Comparison of computed and measured critical gains for structural resonance.

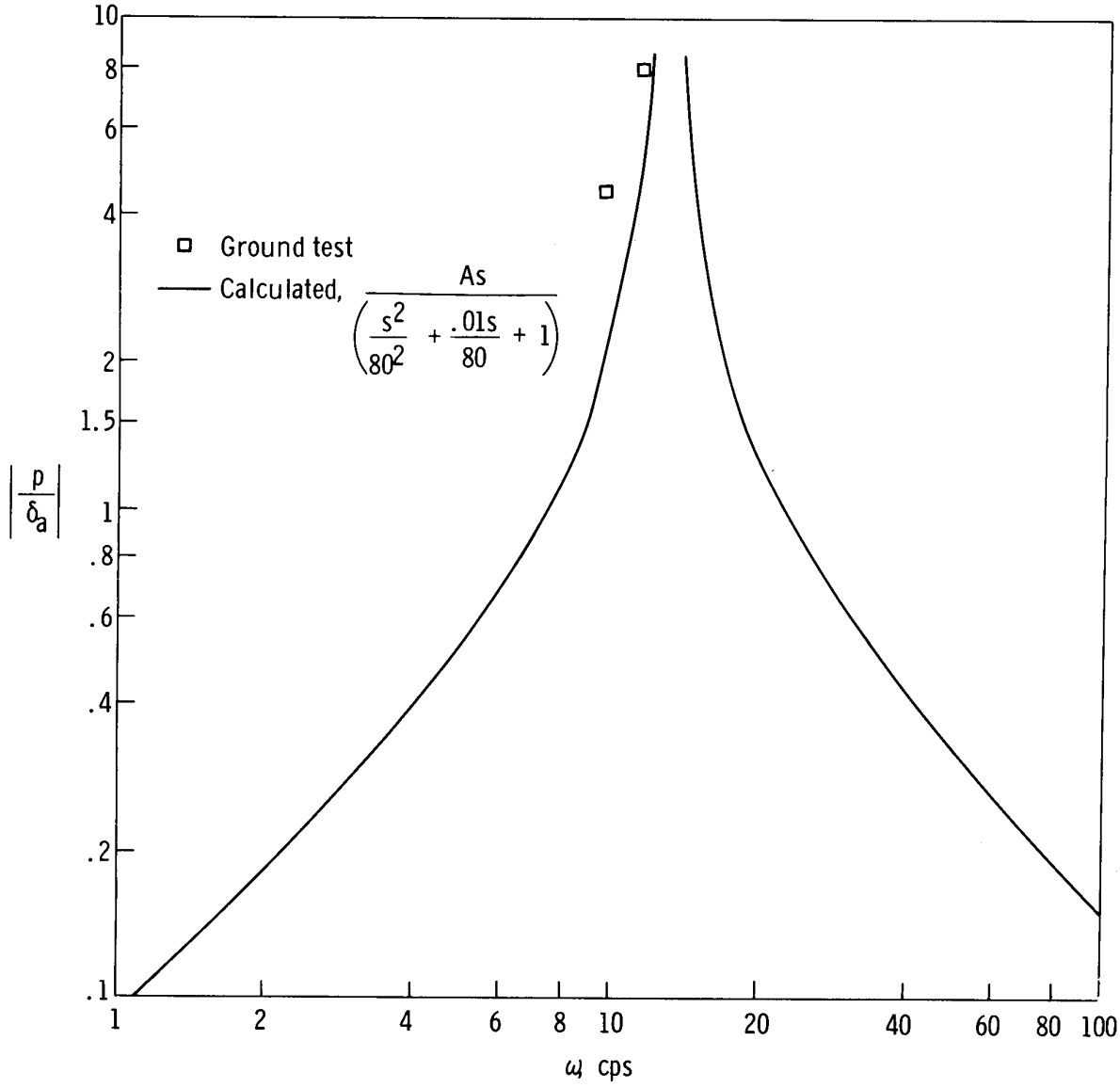

Figure 22. – Comparison of calculated and measured inertial reaction of the fuselage to aileron roll-control-surface acceleration.

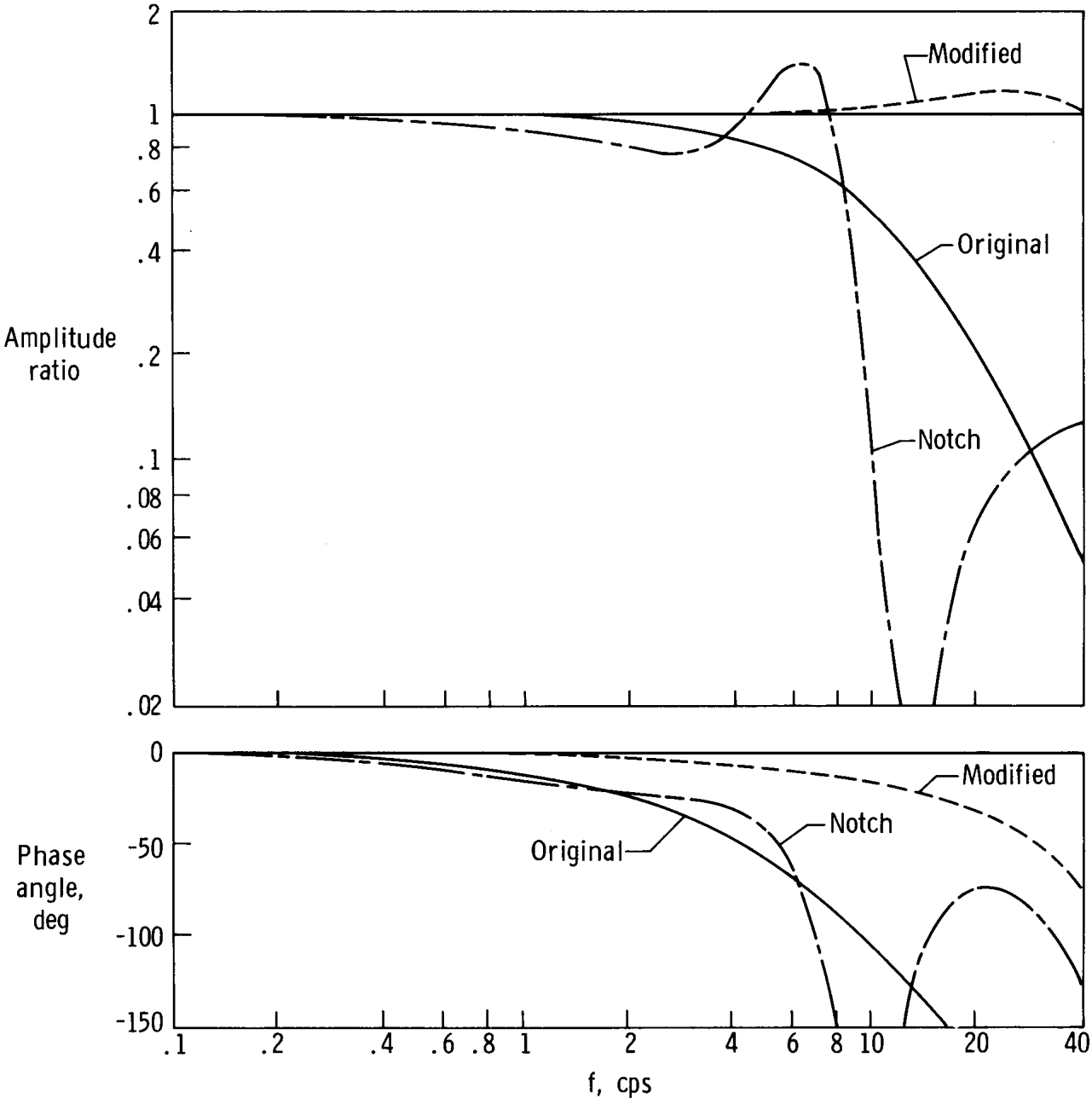

Figure 23. – Frequency response of the original, modified, and notch filters.

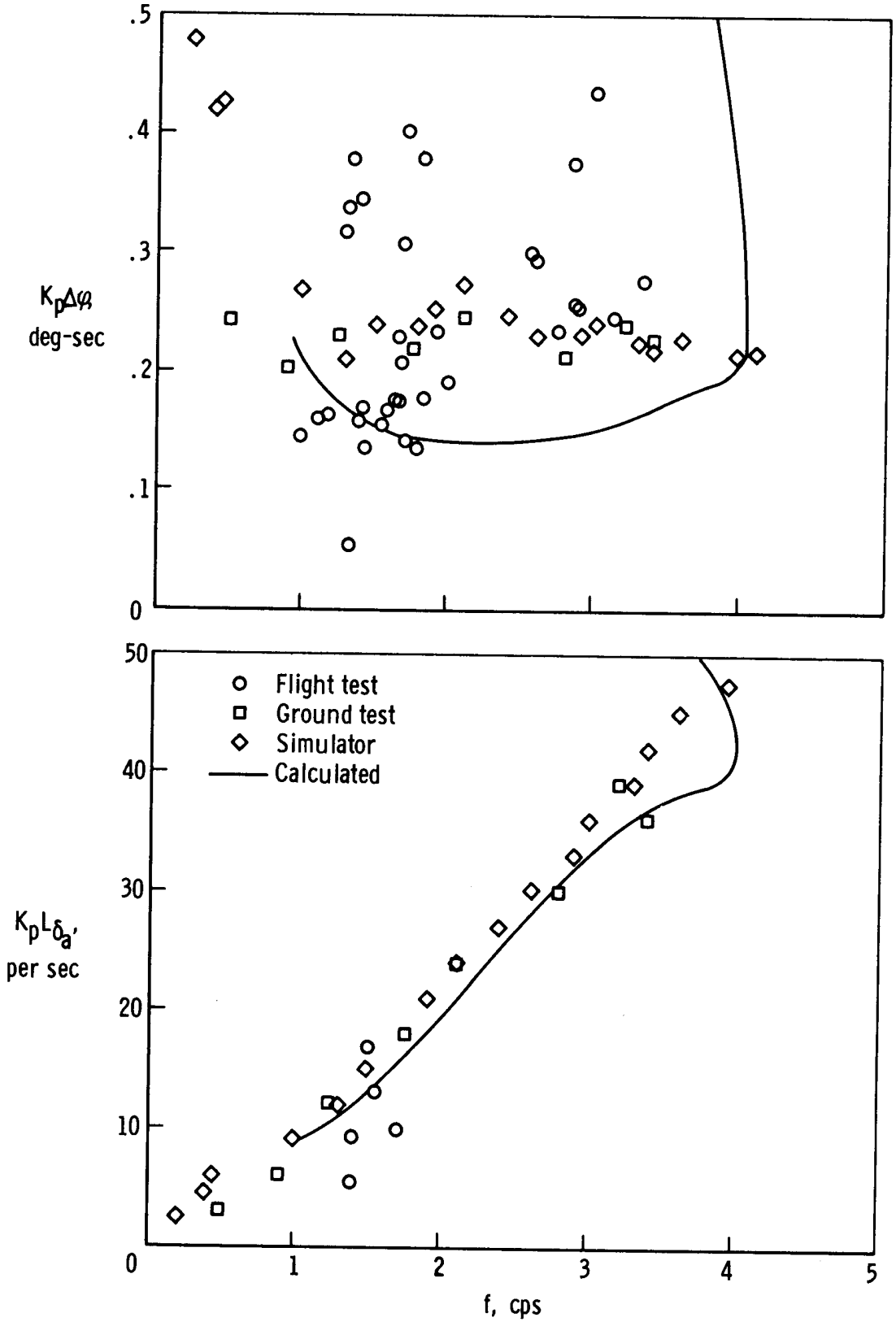

Figure 24. – Comparison of measured and calculated roll limit-cycle characteristics with the notch filter.